NAVAL POSTGRADUATE SCHOOL

MONTEREY, CALIFORNIA

THESIS

NUMERICAL ANALYSIS OF SHEAR THICKENING FLUIDS FOR BLAST MITIGATION APPLICATIONS

by

Zhu, Weijie Kelvin

December 2011

Thesis Co-Advisors: Young W. Kwon
Jarema M. Didoszak

Approved for public release; distribution is unlimited

THIS PAGE INTENTIONALLY LEFT BLANK

REPORT DOCUMENTATION PAGE			Form Approved OMB No. 0704-0188
Public reporting burden for this collection of information is estimated to average 1 hour per response, including the time for reviewing instruction, searching existing data sources, gathering and maintaining the data needed, and completing and reviewing the collection of information. Send comments regarding this burden estimate or any other aspect of this collection of information, including suggestions for reducing this burden, to Washington headquarters Services, Directorate for Information Operations and Reports, 1215 Jefferson Davis Highway, Suite 1204, Arlington, VA 22202-4302, and to the Office of Management and Budget, Paperwork Reduction Project (0704-0188) Washington DC 20503.			
1. AGENCY USE ONLY ***(Leave blank)***	**2. REPORT DATE** December 2011	**3. REPORT TYPE AND DATES COVERED** Master's Thesis	
4. TITLE AND SUBTITLE Numerical Analysis of Shear Thickening Fluids for Blast Mitigation Applications		**5. FUNDING NUMBERS**	
6. AUTHOR(S) Zhu Weijie Kelvin			
7. PERFORMING ORGANIZATION NAME(S) AND ADDRESS(ES) Naval Postgraduate School Monterey, CA 93943-5000		**8. PERFORMING ORGANIZATION REPORT NUMBER**	
9. SPONSORING /MONITORING AGENCY NAME(S) AND ADDRESS(ES) N/A		**10. SPONSORING/MONITORING AGENCY REPORT NUMBER**	
11. SUPPLEMENTARY NOTES The views expressed in this thesis are those of the author and do not reflect the official policy or position of the Department of Defense or the U.S. Government. IRB Protocol number _____N/A____.			
12a. DISTRIBUTION / AVAILABILITY STATEMENT Approved for public release; distribution is unlimited		**12b. DISTRIBUTION CODE** A	

13. ABSTRACT (maximum 200 words)

Improvised Explosive Devices (IEDs) have evolved over the years to become one of the main causes of casualties and fatalities in recent conflicts. One area of research focuses on the improvement of blast attenuation using Shear Thickening Fluid (STF). The STF is a dilatant material, which displays non-Newtonian characteristics in its unique ability to transit from a low viscosity fluid to a high viscosity fluid. Although empirical research and computational models using the non-Newtonian flow characteristics of STF have been conducted to study the effects of STF on blast mitigation, to the author's best knowledge, no specific research has been performed to investigate the STF behavior by modeling and simulation of the interaction between the base flow and embedded rigid particles when subjected to shear stress. The model considered the Lagrangian description of the rigid particles and the Eulerian description of fluid flow. The numerical analysis investigated key parameters such as applied flow acceleration, particle distribution arrangement, volume concentration of particles, particle size, particle shape, and particle behavior in Newtonian and Non-Newtonian fluid base. The fluid-particle interaction model showed that the arrangement, size, shape and volume concentration of particles had a significant effect on the behavior of STF. Although non-conclusive, the addition of particles in Non-Newtonian fluids showed a promising trend of better shear thickening effect at high shear strain rates.

14. SUBJECT TERMS Shear Thickening Fluids, Blast Mitigation, Rigid Body Modeling			**15. NUMBER OF PAGES** 81
			16. PRICE CODE
17. SECURITY CLASSIFICATION OF REPORT Unclassified	**18. SECURITY CLASSIFICATION OF THIS PAGE** Unclassified	**19. SECURITY CLASSIFICATION OF ABSTRACT** Unclassified	**20. LIMITATION OF ABSTRACT** UU

NSN 7540-01-280-5500

Standard Form 298 (Rev. 8-98)
Prescribed by ANSI Std. Z39.18

THIS PAGE INTENTIONALLY LEFT BLANK

Approved for public release; distribution is unlimited

NUMERICAL ANALYSIS OF SHEAR THICKENING FLUIDS FOR BLAST MITIGATION APPLICATIONS

Zhu, Weijie Kelvin
Captain, Singapore Army
B.Eng. (Civil), Nanyang Technological University, Singapore, 2006

Submitted in partial fulfillment of the
requirements for the degree of

MASTER OF SCIENCE IN MECHANICAL ENGINEERING

from the

NAVAL POSTGRADUATE SCHOOL
December 2011

Author: Zhu Weijie Kelvin

Approved by: Young W. Kwon
Thesis Co-Advisor

Jarema M. Didoszak
Thesis Co-Advisor

Knox T. Millsaps
Chair, Department of Mechanical and Aerospace Engineering

THIS PAGE INTENTIONALLY LEFT BLANK

ABSTRACT

Improvised Explosive Devices (IEDs) have evolved over the years to become one of the main causes of casualties and fatalities in recent conflicts. One area of research focuses on the improvement of blast attenuation using Shear Thickening Fluid (STF). The STF is a dilatant material, which displays non-Newtonian characteristics in its unique ability to transit from a low viscosity fluid to a high viscosity fluid. Although empirical research and computational models using the non-Newtonian flow characteristics of STF have been conducted to study the effects of STF on blast mitigation, to the author's best knowledge, no specific research has been performed to investigate the STF behavior by modeling and simulation of the interaction between the base flow and embedded rigid particles when subjected to shear stress. The model considered the Lagrangian description of the rigid particles and the Eulerian description of fluid flow. The numerical analysis investigated key parameters such as applied flow acceleration, particle distribution arrangement, volume concentration of particles, particle size, particle shape, and particle behavior in Newtonian and Non-Newtonian fluid base. The fluid-particle interaction model showed that the arrangement, size, shape and volume concentration of particles had a significant effect on the behavior of STF. Although non-conclusive, the addition of particles in Non-Newtonian fluids showed a promising trend of better shear thickening effect at high shear strain rates.

THIS PAGE INTENTIONALLY LEFT BLANK

TABLE OF CONTENTS

LIST OF FIGURES

THIS PAGE INTENTIONALLY LEFT BLANK

LIST OF TABLES

THIS PAGE INTENTIONALLY LEFT BLANK

ACKNOWLEDGMENTS

I would like to thank my thesis advisor, Professor Young W. Kwon, for his mentorship, advice and supervision throughout the course of this thesis. His ability to guide me through the challenging aspects of the study by going through the fundamentals of the problem patiently was invaluable.

I would also like to thank Professor Jarema Didoszak for his hands-on approach in guiding and helping me with the understanding of my research. His patience and kind understanding had been instrumental in times when I faced any obstacles in my nine months of working on this thesis.

Without the love, support and understanding from my wife, Jean, it would not have been possible for me to complete the thesis. Her unwavering encouragement, together with the joy my two-year-old son, Caleb, brings to me, provided me a huge motivation to achieve the best I could for this study.

Thank God for His wisdom, providence and sustenance in this one year of graduate studies in the Naval Postgraduate School.

THIS PAGE INTENTIONALLY LEFT BLANK

I. INTRODUCTION

A. MOTIVATION AND IMPETUS FOR STUDY

Improvised Explosive Devices (IEDs) have evolved over the years to become one of the main causes of casualties and fatalities in recent conflicts over the past decade. In Afghanistan, the percentage of deaths caused by IEDs had risen steadily from 12% in 2002 to 55% in 2010 according to the Afghanistan Index published by Brookings, which tracks variables of reconstruction and security in Post-9/11 Afghanistan (Livingston & O'Hanlon, 2011). The DoD Personnel and Military Casualty Statistics also attributed 70% of all American combat casualties in Iraq to IED attacks. With IEDs likely to continue to be a weapon of choice among terrorists and insurgents, due to the relative ease of obtaining and assembling their components, a multi-dimensional approach will be required to counter the threat. Besides formulating a robust tactical strategy to defeat the employment of IEDs against the security forces, investment in counter-IED technologies remains a viable alternative in reducing the vulnerability of troops towards the threat.

Counter-IED technologies include electronic jammers, radars, X-ray equipment, robotic explosive ordnance disposal equipment, physical security equipment, and armor for vehicles and personnel (Wilson, 2006). Specific to the area on armor for vehicles and personnel, technological advancement focuses on blast mitigation, which includes further fields of energy absorption, energy dissipation, and energy channeling capabilities of the protective structure. To keep pace with protection levels provided by ballistic armor research, there has been a shift in recent protective studies on energy dissipative materials and systems to protect human bodies against explosive overpressures.

Different types of energy dissipative materials have been studied. They include multi-composites sandwich panels, 'soft' condensed matter such as

granular materials or foams (Nesterenko, 2003), and non-Newtonian fluids such as the Shear Thickening Fluid (STF).

The Shear Thickening Fluid has been well researched in terms of its capability in enhancing the performance of body armor against ballistic impact (Lee & Wagner, 2003) and for stab-resistance (Decker & Wetzel, 2007). However, an area in which more could be studied is the potential effects of STF on shock and blast wave mitigation. The motivation herein is to harness the strength of the STF while being able to be flexibly deployed and relatively easily transportable, yet able to withstand and dissipate pressure wave loading when required.

The study also adopted a numerical analysis approach in examining the behavior of the Shear Thickening Fluid using Lagrangian models in Computational Fluid Dynamics (CFD) software so that the dynamics of the interactions could be studied at the particle level, and particle parameters could be varied. While computer simulations had contributed significantly to the study of the mechanism of shear thickening, only Eulerian CFD models had been used in research so far to study the specific behavior of Non-Newtonian Fluids, such as the Shear Thickening Fluids (Petkova et al., 2003) and the Shear Thinning Fluids (Ein-Mozaffari & Upreti, 2010). Other computer models used various techniques such as the Stokesian Dynamics techniques (Foss & Brady, 2000), the Dissipative Particles Dynamics (Boek et al., 1997) and the Lagrange Multiplier Fictitious Domain Method (Glowinski et al., 1999), to simulate particle behavior in suspensions for particulate or granular flows. Lagrangian models would offer a different dimension of studying the STF. The CFD model could also be used to investigate cases where it would not be easy to obtain experimentally.

B. LITERATURE REVIEW

1. Non-Newtonian Fluid (NNF)

A Newtonian fluid is a fluid that displays linearity relationship between the stress and strain rate. The constant of proportionality is known as viscosity. An equation to describe Newtonian fluid behavior is

$$\tau = \mu \frac{du}{dy}$$

where τ is the shear stress exerted by the fluid;

μ is the fluid viscosity;

$\frac{du}{dy}$ is the strain rate, or the velocity gradient perpendicular to the direction of shear.

Figure 1 shows the mentioned relationship and compares between the Newtonian and non-Newtonian fluids, such as the Shear Thickening Fluid and the Shear Thinning Fluid. The Newtonian Fluid shows a linear relationship between shear stress and shear strain rate. The shear thickening effect of the STF is illustrated by the lower rate of increase in shear stress at low shear strain rate regions, while increasing at a higher rate at high shear strain rate values. The converse is true for the Shear Thinning Fluid.

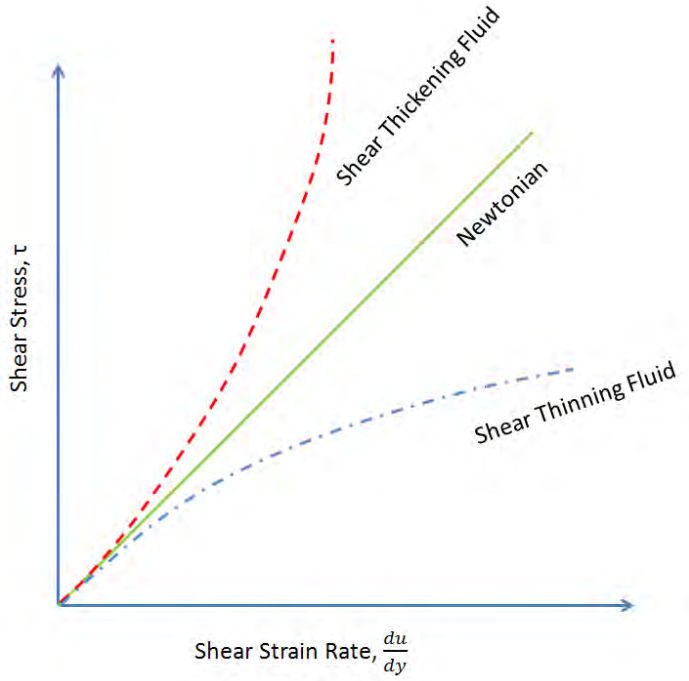

Figure 1. Shear Stress and Shear Strain Rate Relationship

A Non-Newtonian Fluid is a fluid whose flow properties differ from that of the Newtonian fluid described above. The viscosity of the NNF is not independent of shear rate or shear rate history. When the viscosity of a fluid decreases with increasing shear rate, the fluid is called shear-thinning. On the other hand, when the viscosity increases as the fluid is subjected to a high shear rate, the fluid is called shear thickening. Examples of NNF include industrial lubricants that are pumped into oil wells to improve oil recovery, household items such as paint, and also blood.

One of the most widely used form of a general non-Newtonian model to describe NNF is the Power-Law Model. It is also called the Ostwald-de Waele relationship. The mathematical relationship is given by

$$\tau = K\left(\frac{du}{dy}\right)^n$$

where K is the flow consistency index;

n is the flow behavior index.

The quantity

$$\mu_{apparent} = K\left(\frac{du}{dy}\right)^{n-1}$$

represents an apparent or effective viscosity as a function of the applied shear rate.

For a Newtonian fluid, the flow behavior index, n, is equal to unity, and the flow consistency index, *K*, is equal to the viscosity for the fluid. For the Shear Thickening Fluid, n is greater than one. The relationship is summarized in Figure 2 where a Newtonian fluid shows a constant Flow Consistency Index value at all levels of shear stress. For the STF, the Flow Consistency Index increases exponentially as the shear stress increases.

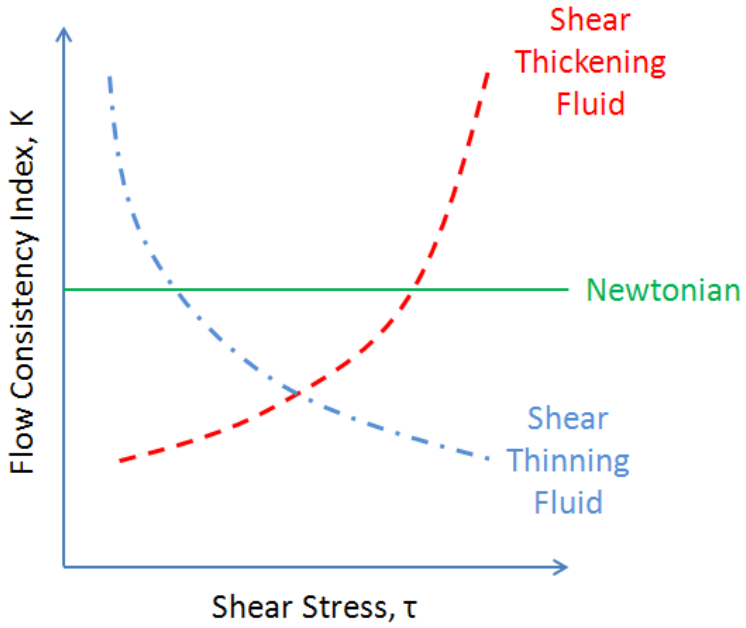

Figure 2. Shear Stress and Flow Consistency Index Relationship

2. Shear Thickening Fluid (STF)

Shear Thickening Fluid is a dilatant material, which displays non-Newtonian characteristics. The material is typically made up of particles such as silica or silicon dioxide, as shown in Figure 3, dispersed in a fluid base, which can be Newtonian in nature, such as water or Polyethylene Glycol (PEG).

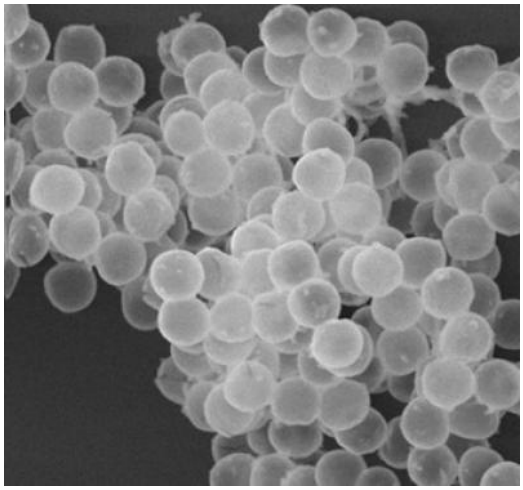

Figure 3. Silica (From microparticles.de)

In STFs, the particles dispersed within the colloid are usually smaller and will not settle like the case of sedimentation of larger solids. This is due to the fact that the particles are subjected to Van der Waals forces evident between mostly spherical particles as the dominant force compared to the gravitational pull (Hamaker, 1937). The magnitude of the effects of these forces have on the particles is inversely proportional to the size of these particulates where gravitational forces are greater than particle-particle interactions for large particulates, and the opposite being true for small particulates.

Dilatancy in a colloid or its ability to order in the presence of shear forces is dependent on the ratio of inter-particle forces. As long as the inter-particle forces such as Van-der-Waal forces dominate, the suspended particles remain in ordered layers. However, once shear forces dominate, particles enter a state of flocculation and are no longer held in suspension. They begin to behave like

solids. When the shear forces are removed, the particles spread apart and once again form a stable suspension.

When shearing a concentrated stabilized solution at a relatively low shear rate, the repulsive particle-particle interactions keep the particles in an ordered, layered, equilibrium structure. However, at shear rates elevated above the critical shear rate, the shear forces pushing the particles together overcome the repulsive particle interactions, forcing the particles out of their equilibrium positions. This leads to a disordered structure, causing an increase in viscosity. The critical shear rate is defined as the shear rate at which the shear forces pushing the particles together are equivalent to the repulsive particle interactions.

One of the key characteristics of the STF is the behavior where dynamic viscosity increases with an applied shear stress. The dilatant effect occurs when closely packed particles are combined with enough fluid to fill the gaps between them. At low velocities, the fluid acts as a lubricant, and the dilatant flows easily. At higher velocities, the liquid is unable to fill the gaps created by the particles, and friction greatly increases, causing an increase in viscosity. STF is also non-Newtonian in nature where its viscosity is not dependent on shear rate or shear rate history. This behavior is one type of deviation from Newton's Law, and is controlled by factors such as particle size, shape and distribution. Empirical studies have also shown that the shear thickening effects would differ due to the different concentration of particles and additives, as well as the molecular chain of the additives (Xu et al., 2010). The larger the concentration of the additive, the more obvious the shear thickening effect. Similarly, the longer the molecular chain of the additive, the stronger the non-Newtonian behavior. It was also discovered in a similar study that energy dissipation is also greater with a larger additive concentration and longer chain of additives.

3. Current State of Research

a. STFs for Ballistic Protection and Stab Resistance

High strength and high modulus fibers have since revolutionized the design of light-weight armor (Jacobs & van Dingenen, 2001). High performance fibers used in ballistic products are often characterized by low density, high strength, and high energy absorption capability. However, due to the dependency on the physical characteristics of the polymeric fibers, there would be a trade-off to ballistic protection with the weight incurred. Shear Thickening Fluid had been used to impregnate protective materials such as Kevlar to form composites for better ballistic protection performance, often resulting in a more flexible and less bulky material, which could be used for body armor (Lee et al., 2002). At low strain rates, associated with the normal motion of the wearer, the fluid would offer little impediment to the fabric deformation and flexure. However, at high strain rates associated with a ballistic impact event, the STF would thicken and in doing so, enhance the ballistic protection of the composite fabric. It was found in the empirical study that energy absorption was found to be proportional to the volume fraction of the STF.

Stab mechanisms are generally classified into puncture and cut (Egres Jr et al., 2004). Puncture refers to impact by instruments with a sharp tip but no cutting edge. On the other hand, a cut refers to impact by knives with a continuous cutting edge. The STF-treated Kevlar and Nylon fabrics were found to exhibit dramatic improvements in puncture resistance under high-speed loading conditions, while slight increases in cut protection were also observed (Decker et al., 2007). The addition of the STF primarily reduced the mobility of the fabric filaments and yarns in the impact zone and microscopy showed significant energy dissipation that involved plastic flow of polymeric filaments, as well as deformation of the filaments due to mechanical interaction with the colloidal particles of the STF.

b. Blast Wave Propagation and Mitigation

The primary damage mechanism of IEDs is through the generation of a blast wave which can adversely affect targets through shock and impulsive loads. An effective analysis and design of protective materials against blast loads thus requires a detailed understanding of the blast phenomena, as well as the dynamic response of the impact target.

According to the Unified Facilities Criteria (UFC) on Structures to Resist the Effects of Accidental Explosions (UFC 3-340-02) which qualifies the blast phenomena, the explosive detonation involve a very rapid and stable chemical reaction which proceeds the explosive material at a supersonic detonation velocity ranging from 22,000 to 28,000 feet per second. The detonation wave rapidly converts the solid or liquid explosive into a very hot, dense and high-pressured gas. The volume of the gas is then the source of strong blast waves in air. Pressures immediately behind the detonation front range from 2,700,000 to 4,900,000 psi. The blast effects of an explosion are in the form of a shock wave composed of high-intensity shock front, which expands outward from the surface of the explosive to the surrounding air. As the wave expands in air, the front impinges on the target surface within its path. The magnitude and distribution of the blast loads are a function of the explosive properties of the material used, the location of detonation, and whether the blast is confined or unrestricted.

The blast mitigation strategies developed to counter the effects of shock loading include the continuity of structures, redundancy in load bearing paths, reserve strength in excess of live loads, increased energy absorbing capabilities and increased building component mass (Kambouchev, 2007). The majority of these concepts are based on increasing the energy dissipation capabilities of the structure and its components.

C. PROPOSED VALUE-ADDED OF STUDY

1. Model for Evaluating the Effects of STF under Blast Loading

Shear Thickening Fluid had been extensively researched for use in impregnation of protective materials in ballistic protection and stab resistance. However, the design parameters for ballistic protection and pressure wave (blast) mitigation are inherently different. Improved impact resistance does not lead to improved pressure wave attenuation. Pressure wave typically causes Traumatic Brain Injury (TBI) (Warden, 2006) and concussion to internal organs (Mernoff & Correia, 2010). The Shear Thickening Fluid resists this type of injuries by reducing the pressure exerted on the body or platform carrying the personnel. This technology has widespread applicability to the IED problem, with body armor, explosion suppression blankets, and vehicle body panels as potential end products.

Until today, empirical analysis seemed to be the research approach of choice for the Shear Thickening Fluid. This was largely due to the high computational cost and time required for modeling of the STF at the particle level. However, with the available experimental data further emphasizing the importance of the STF in blast mitigation technologies, it seem logical to invest in modeling and studying the material numerically to fully exploit the natural phenomenon and its strength in providing better blast protection.

2. Optimal Material Configuration for STF

From the results of the numerical analysis on the effects of particle size, particle distribution, particle shape and volume concentration of particles in the fluid on the blast mitigation performance of the Shear Thickening Fluid, the report aimed to recommend an optimal material configuration based on the computational results.

D. MODELING AND COMPUTATIONAL FLUID DYNAMICS (CFD)

1. Overview of CFD

Computational Fluid Dynamics is a branch of fluid mechanics that uses numerical methods and algorithms to solve and analyze problems that involve fluid flows (Anderson, 1995). The technique presumes that the equations that govern the physical behavior of a flow system are known, in the form of Navier-Stokes, thermal energy and the appropriate equations of state. The equations are obtained by requiring the mass, momentum, thermal energy, and species concentration be conserved locally and globally within the model (Ladeinde & Nearon, 1997).

In almost all CFD approaches, the geometry and boundary conditions are defined during pre-processing. The plane or volume occupied by the fluid is then divided into discrete cells, otherwise known as meshes. These meshes may be uniform or non-uniform. For transient problems, the initial conditions are also defined. The simulation is subsequently started and the equations would be solved iteratively until a specific pre-determined time is reached or a specified solution convergence limit is achieved. A post-processor would be used for the analysis and visualization of the resulting solution generated.

2. Available CFD Codes

ANSYS is a computer-aided engineering simulation software package that calculates flow fields and other physics in detail for an application of interest. It uses a multidisciplinary approach in simulation in which fluid flow models integrate with other types of physics simulation technologies (ANSYS, 2011). One well-known product offered by ANSYS is the ANSYS CFX.

The ANSYS CFD solvers are based on the finite volume method (ANSYS, 2010). The domain is discretized into a finite set of control volumes and general conservation equations for mass, momentum, energy and species are solved on the set of control volume. The partial differential equations are discretized into a

system of algebraic equations which are subsequently solved numerically to render the solution field. The CFX control volumes are node-centered.

The ANSYS CFX solver uses coupled algebraic multigrid to achieve its solutions and its engineered scalability ensures a linear increase in CPU time with problem size and parallel performance. The CFX also allows maximum interaction among physical models with all elements types and across grid interface connection types to allow comprehensive multi-physics simulations. For multiphase simulation, it uses the Lagragian transport model that allows solution of particle phase within a continuous phase. It also contains the Eulerian multiphase model to capture the exchange of momentum, energy, and mass. Furthermore, it is also incorporated with advance solvers such as the Rigid Body Solver which can model the Lagrangian effects of rigid bodies in fluid flow.

3. Advantages of CFD

CFD Analysis complements testing and experimentation by reducing the total effort and cost required for empirical data acquisition. This is assisted by the relatively cheaper cost of computing and improvement in the computational power for complicated problems. Having examined the advantages of CFD, it does not exclude the need for experimentation to validate the codes used for the modeling of the problem description, which is important for any numerical analysis.

E. MODELING APPROACH

1. Eulerian and Lagrangian Modeling

Challenges exist when modeling multiphase flows such as the Shear Thickening Fluid due to the complex interaction between phases. Formulation of proper constitutive relations is key in correctly predicting flow behavior. For modeling of granular flows like the STF, several approaches can be adopted. One approach is the Eulerian-Lagrangian Model where the trajectories of the particles are modeled in a Lagrangian frame. Another approach is the Eulerian-

Eulerian Model which models both the fluid base and the particles as continuous Eulerian phases.

The Eulerian methodology uses only particle concentration equations to couple with momentum and turbulence equations, with the one-way coupling of flow to particles. The model treats the particle phase as a modified scalar species and the particle phase follows the following transport equation:

$$\frac{\partial \rho C}{\partial t} + \frac{\partial}{\partial x_i}(\rho \bar{u}_i C - \Gamma \frac{\partial C}{\partial x_i}) = S_C$$

where t is time;

C is the particle concentration;

ρ is the density of air;

x_i is the three coordinates (i = 1, 2, 3);

$\bar{u}_i$ is the average velocity components in the three directions;

Γ is the particle diffusivity;

S_c is the particle source term.

The particle diffusivity is also described as

$$\Gamma = \rho\ (D + v_p)$$

where D is the Brownian diffusivity of particles;

v_p is the particle turbulent diffusion coefficient.

When the particle size is larger than 0.01 μm, the Brownian diffusivity is negligible compared with turbulent diffusivity in a turbulent flow.

The Lagrangian method usually tracks transiently a large number of particles. The method starts from solving the transient momentum equation of each particle:

$$\frac{d\vec{u}_p}{\partial t} = F_D(\vec{u} - \vec{u}_p) + \frac{\vec{g}(\rho_p - \rho)}{\rho_p} + \vec{F}_a$$

where $\vec{u}_p$ is the particle velocity vector;

F_D is the inverse of relaxation time;

$\vec{u}$ is the fluid velocity;

ρ and ρ_p are the density of fluid and particles respectively;

$\vec{F}_a$ is the additional forces.

The numerical calculation procedure for the Eulerian and Lagrangian models are very different as they are developed in different frames of reference (Zhang & Chen, 2006). In steady state conditions, the Eulerian method requires many iterations to obtain a converged concentration field of particles. The Lagrangian method tracks particles trajectories in a manner of time matching and needs to repeat the simulation many times to obtain a stable solution. In a transient solution, the particle concentration equation in the Eulerian method is solved along with the flow equations at each time step. Iterations are necessary at each time step to ensure convergence. For the Lagrangian method, particles are tracked at the end of each time step when the flow computation is converged. At the same time, the particle positions are recorded and the particle concentration is computed.

2. Rigid Body Modeling

A rigid body is defined as a solid object that moves through a fluid without itself deforming (EDR, 2011). The fluid forces and external forces, if any, dictates the motion of the rigid body. A rigid body is defined by a collection of two-dimensional regions that form its faces. The solver does not require the rigid body to be meshed and mesh motion is used to move rigid body faces in accordance with the rigid body equations of motion.

Simulating the motion of a rigid body is similar to simulating the motion of a particle (Baraff 2001). In addition to the definition of particles, rigid bodies have rotations, as well as a volume of space and a particular shape. A function

II. NUMERICAL ANALYSIS

A. MODELING OF SHEAR THICKENING FLUIDS

Most modeling of Shear Thickening Fluids like blood or industrial slurries have been modeled using a two-phase or multi-phase Eulerian approach. However, the Eulerian model could only provide an overall performance of the fluid, which contains both the fluid base and the particulates as dual-phases. The model would only allow the variation of general particulate properties in a defined phase, as well as the change of volume concentration based on the volume fraction determined.

In order to achieve the proposed value-added of this study, a Lagrangian approach was adopted to analyze the performance of the STF at the particle-level, based on interaction with an Eulerian fluid base. The Lagrangian methodology allowed the tracking of particle movements when subjected to shear forces. It also allowed the investigation of the behavior of the particles based on the user-defined distribution and size.

As the numerical analysis focused on the behavior of each individual particle, the ANSYS CFX Rigid Body Solver was used to analyze the particles at micro-level, allowing each rigid body to model the movement of every particle subjected to shear loading.

The ANSYS CFX software was chosen to do the simulation due to its ability to handle fluid flows at both an Eulerian and Lagrangian level, as well as having the integrated rigid body solver to handle the particles displacement and disposition. Solidworks was the mechanical Computer-Aided Design (CAD) program used to create the model for the geometric input into CFX. Solidworks is a parasolid-based solid modeler and utilizes a parametric feature-based approach to create models and assemblies (Solidworks, 2011).

The numerical analysis was conducted in the following stages:

- A single stationary particle in a fluid base control volume

- Multiple stationary particles in the same control volume
- A fully populated particulate system
- A single rigid body particle subjected to movement in a fluid base control volume
- Multiple rigid body particles subjected to movement in a fluid base control volume
- Variation of particle and fluid parameters based on the STF model

B. MODELING PROCEDURE

This section documents the computational fluid dynamics modeling procedure and the considerations for the choice of methodology to achieve as high fidelity as possible in the model.

1. Geometric Inputs

To model the fluid base and particles of the Shear Thickening Fluid, the geometric inputs of the model involved drawing the fluid domain using Solidworks. The particles were created by having extruded cuts on the desired particle positions in the fluid domain, usually the starting position of the particles at the initialization stage of the modeling. For Rigid Body Modeling in the latter stages of the modeling, a sub-domain was also created for each rigid body to allow modeling of the motion of the particle. The sub-domains were defined such that it did not interfere with the projected motion of the particles.

Although the study focused on a two-dimensional model, a three-dimensional model had to be defined with a single cell thickness on the z-dimension as required by CFX for meshing and analysis.

The control volume was chosen to allow sufficient development of the shear flow to see the reaction of the particle or particles involved to the forced applied. A control volume that was too small would see the boundary conditions interfere with the movement of the particles early on in the simulation, which was not desirable. A control volume that was not large would not accurately model the

type of shear force acting the particles, as would a blast pressure loading on a particulate system.

2. Meshing

A hexahedral mesh (quadrilateral in two directions), as shown in Figure 4, was used to define the three-dimensional model. Compared to tetrahedral meshes (triangular in 2-D), a hexahedral mesh offers a lower element count but allows directional sizing without loss of accuracy.

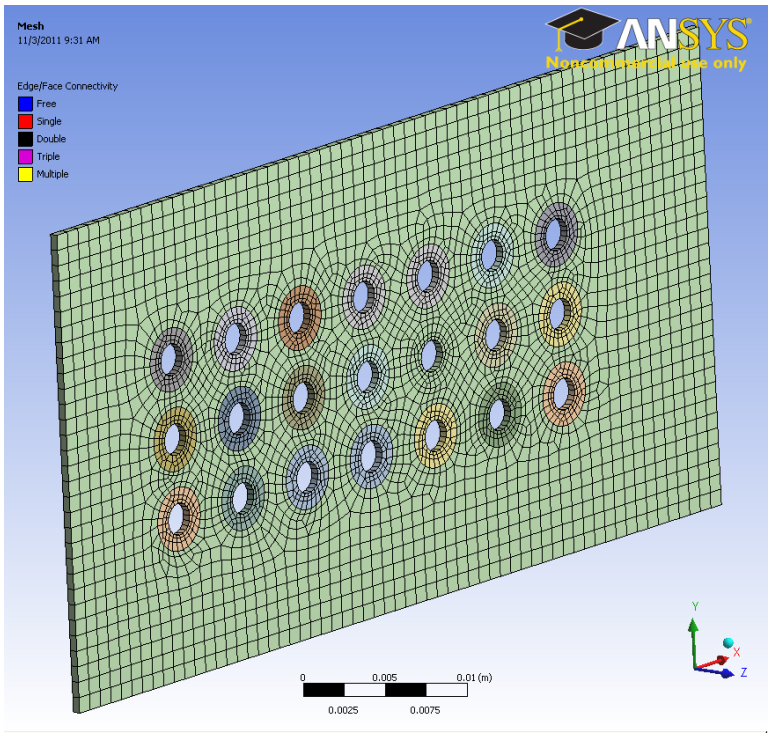

Figure 4. Hexahedral Mesh

3. Transient Modeling

The objective of the study required the modeling to be transient, in order to observe the behavior of the particles at various time steps when subjected to a shear loading. Transient simulations were solved by computing the solution for many discrete points in time, and at each point, iterations called coefficient loops were performed to obtain a solution. The time step size was selected to allow

sufficient resolution in observing time dependent data such as displacement of particles and force exerted on particles at a particular time step. An initial condition was required to define the start state of the simulation.

A total time duration of 2 s and a time step of 0.01 s was selected for this study. The transient time frame was chosen based on the size of the particles of diameter of 1 and 2 mm, and control volume of 0.06 m by 0.025 m, as well as the applied flow acceleration of 0.1 to 0.4 m/s^2. It would allow the observation of the critical behavior of the Shear Thickening Fluid when subjected to a short duration of shear loading typical to a blast pressure wave.

4. Materials

The fluid base of the Shear Thickening Fluid is typically a Newtonian fluid. In the model, water with a viscosity of 8.90×10^{-4} Pa.s was used.

Sand particles were used for the material properties of the particles placed inside the fluid base. A uniformly shaped spherical particle, with a baseline diameter of 2mm, was also modeled as a rigid body in the model to limit the variability of the parameters examined in the study.

5. Boundary Conditions

Boundary conditions were important in defining the model and ensuring the correct conditions were enforced for the study. The study required a shear force being applied on the fluid domain, containing the pre-determined particle distributions.

A shear force was applied by defining an inlet on the upper boundary and applying a shear velocity on the *u* component of the Cartesian velocity components. The bottom boundary was defined as a no slip wall condition to achieve the shear development of the flow between the top and bottom boundaries. Since the shear fluid flow would require a long channel to be fully developed, periodic boundary conditions were applied to the left and right interfaces. As CFX does not have a separate 2-D and 3-D solver, it could not

read planar or 2-D meshes. Thus in the meshing, a thin 3-D volume was created with a single cell thickness, and symmetry boundaries were applied to the front and back faces of the control volume created.

The Rigid Body Solver required the 2-D interfaces of the extruded cut particles be defined as walls since it did not allow mesh deformation. The mesh motion for the Rigid Body boundary interfaces was set to “Rigid Body Solution”, instead of the default setting of “Stationary”. The conditions are as shown in Figure 5.

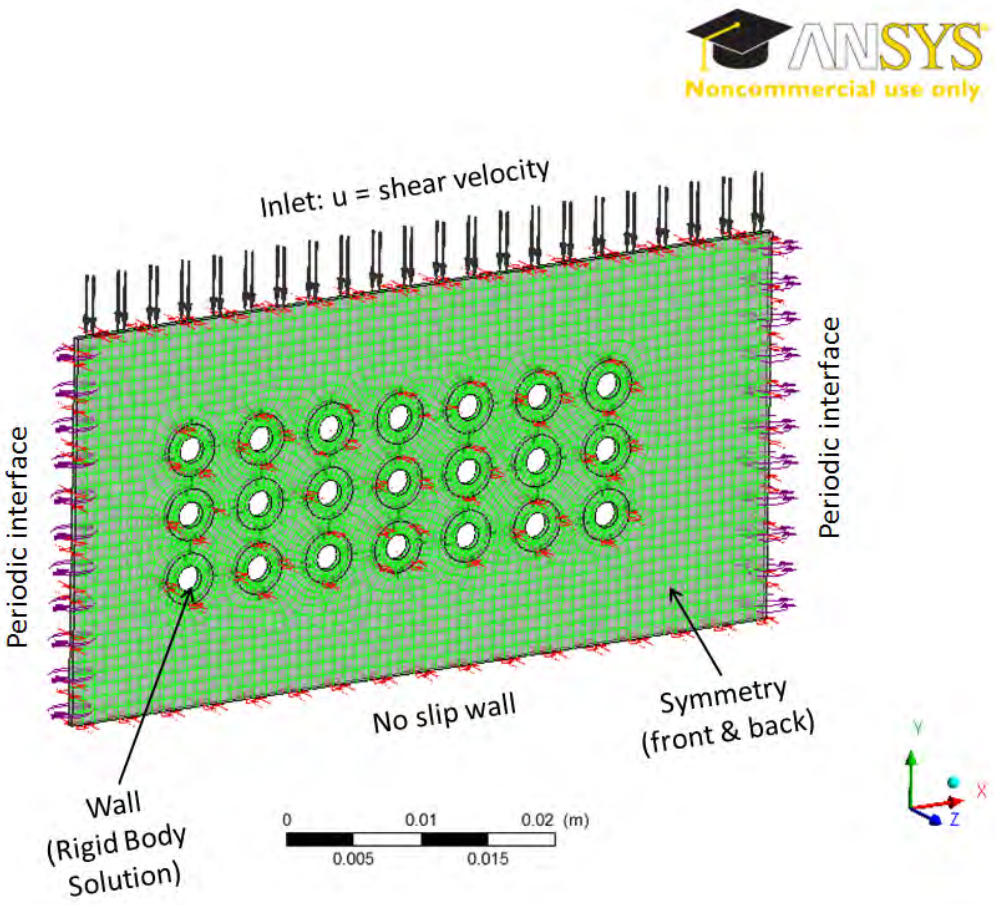

Figure 5. Boundary Conditions

C. MODELING OF STATIONARY PARTICLES IN A CONTROL VOLUME

A single stationary particle, as shown in Figure 6, was first modeled to study the effects of a particle in the control volume under shear flow conditions.

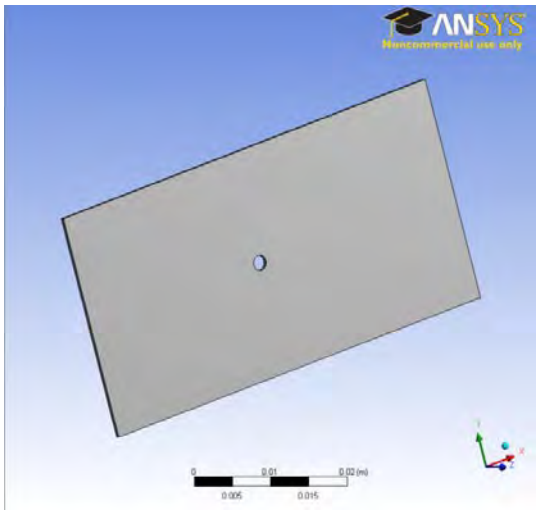

Figure 6. Single Stationary Particle Model

The transient velocity plots shown in Figure 7 sampled every 0.1s showed a consistent reduction of velocity at the locality of the particle at the center of the control volume.

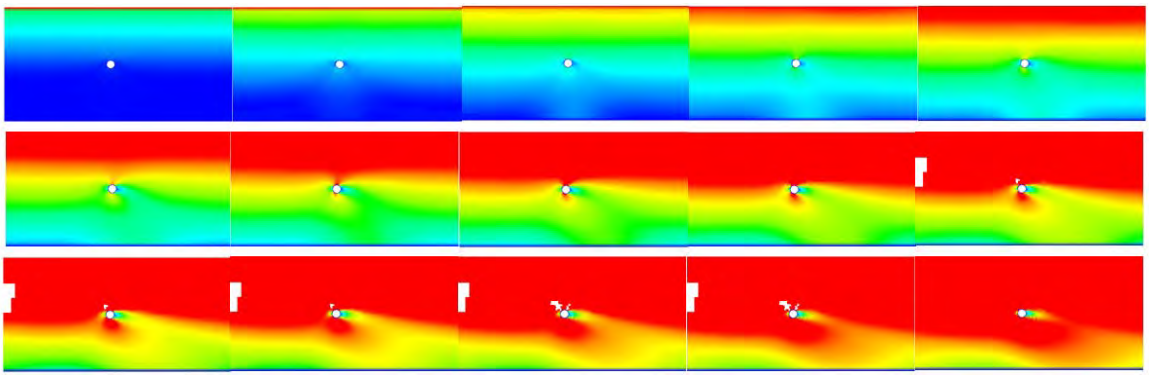

Figure 7. Transient Velocity Plot of Single Stationary Particle

Two more particles, as shown in Figure 8, were subsequently added to the control volume to study the effects of a group of particles on the shear flow. The behavior was similar to that of a single particle modeling where the velocity of the

flow was observed to decrease around the particle, and leaving a visible wake relative to the direction of the shear flow.

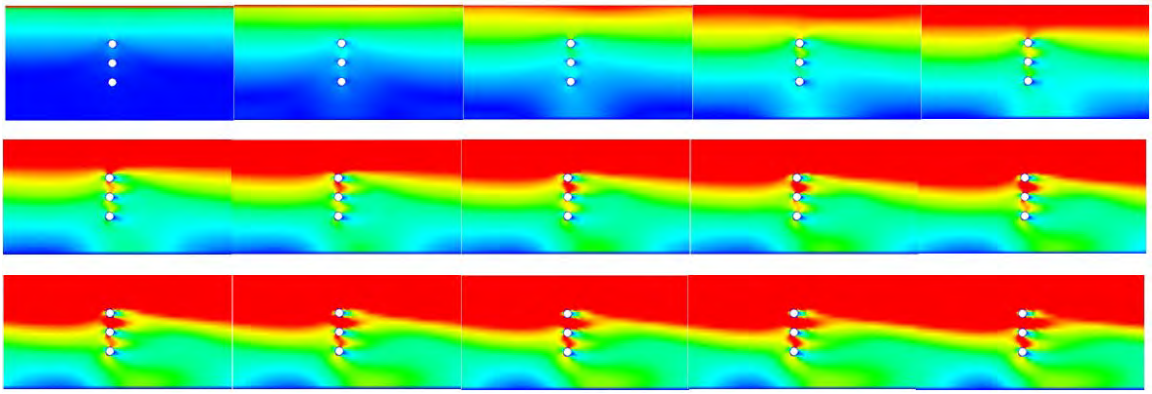

Figure 8. Transient Velocity Plot of Three Stationary Particles

The number of particles was subsequently increased to populate the entire fluid domain as shown in Figure 9 in order to observe any interaction among the particles. With the shear velocity applied and total time of simulation unchanged, it was observed that the increase of velocity based on the same depth of

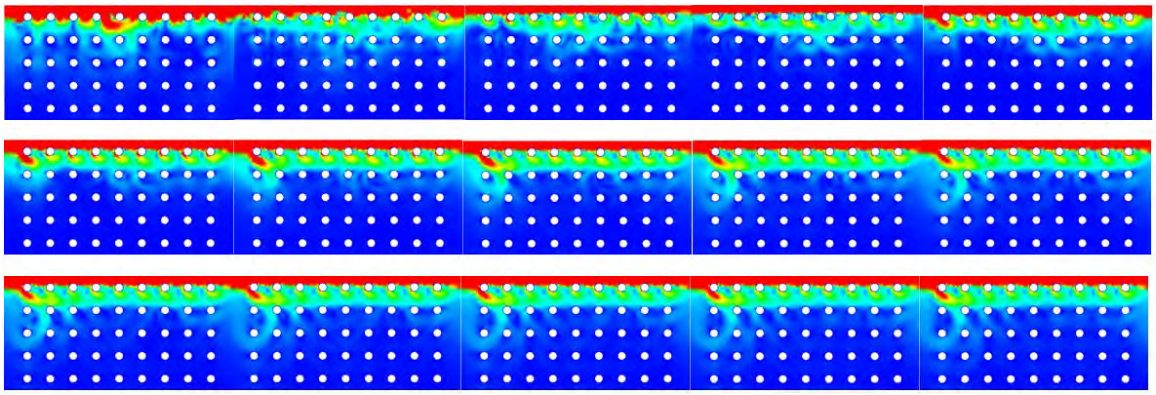

D. MODELING OF PARTICLES USING THE RIGID BODY SOLVER

To model the particles as separate rigid bodies, a subdomain had to be defined for each particle to allow mesh deformation based on the outputs of the Rigid Body Solver. This could be seen in Figure 10 which shows the colored circular offsets around the extruded cut rigid bodies in the control volume. Each particle had to be separately modeled as their behavior would be independent of one another, when subjected to external forces at different start state locations.

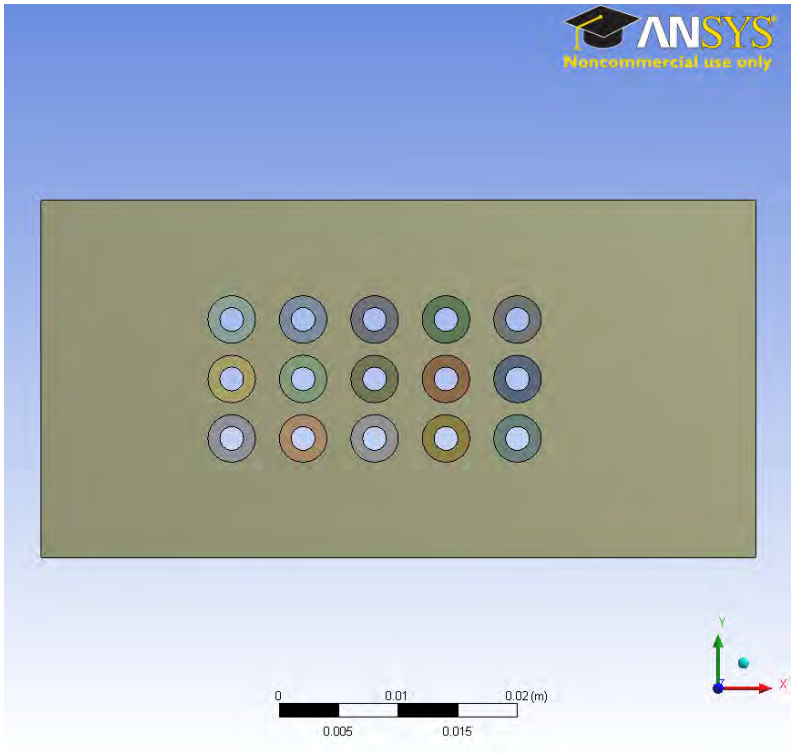

Figure 10. Sub-Domain for Each Rigid Body

When the rigid bodies were allowed to translate, the behavior of the entire domain, consisting the fluid domain and the rigid body particles, would be more realistically modeled when subjected to shear forces. However, in order to investigate the shear effects on the particles, the gravity effects on the particles were eliminated so that the study could concentrate on the pure shear effects and reactions.

Due to the limitation of the CFX solver for handling large mesh deformation, the modeling had to be truncated when the limit specified in the mesh solver was reached. If the deformation of the mesh elements due to the moving particles is too large, it would be difficult to allow mesh deformation for the initial meshing without destroying or distorting the mesh elements. Thus, the results to be presented were evaluated based on the pre-truncated simulation runs as determined by the deformed mesh elements.

E. PARAMETERS OF PARTICLES FOR MODELING

The following variables were chosen and separately modeled to study the effects of the shear thickening fluid:

- Applied Flow Acceleration on the Control Volume
- Particle Distribution Arrangement
- Volume Concentration of Particles
- Particle Size
- Particle Shape
- Particles in Non-Newtonian Fluid

The shear stress and shear strain rate of the model STF were subsequently measured, and the results of the modeling were documented in Section III of the report. The numerical data extracted from the modeling can be found in Appendix A.

THIS PAGE INTENTIONALLY LEFT BLANK

III. RESULTS

A. CHANGE IN APPLIED FLOW ACCELERATION

Four different shear velocities were applied at the top boundary of the control volume to determine the behavior of the Shear Thickening Fluid when subjected to different magnitude of flow acceleration. Velocities of 1 m/s, 2 m/s, 3 m/s and 4 m/s were applied in the horizontal component of the velocity at the top boundary to model a shear flow across the control volume on the STF. The velocity applied at the top boundary increased from zero to the specified velocity with an acceleration, and the average accelerations are shown in Figure 11. The flow acceleration was obtained by taking the gradient of the velocity-time graph in Figure 11. The average flow acceleration achieved for velocities of 1 to 4 m/s are 0.096911 m/s^2, 0.19459 m/s^2, 0.300903 m/s^2 and 4.24671 m/s^2 respectively. The flow acceleration for the respective flows would be simplified and named as 0.1 m/s^2, 0.2 m/s^2, 0.3 m/s^2 and 0.4 m/s^2 henceforth in the report.

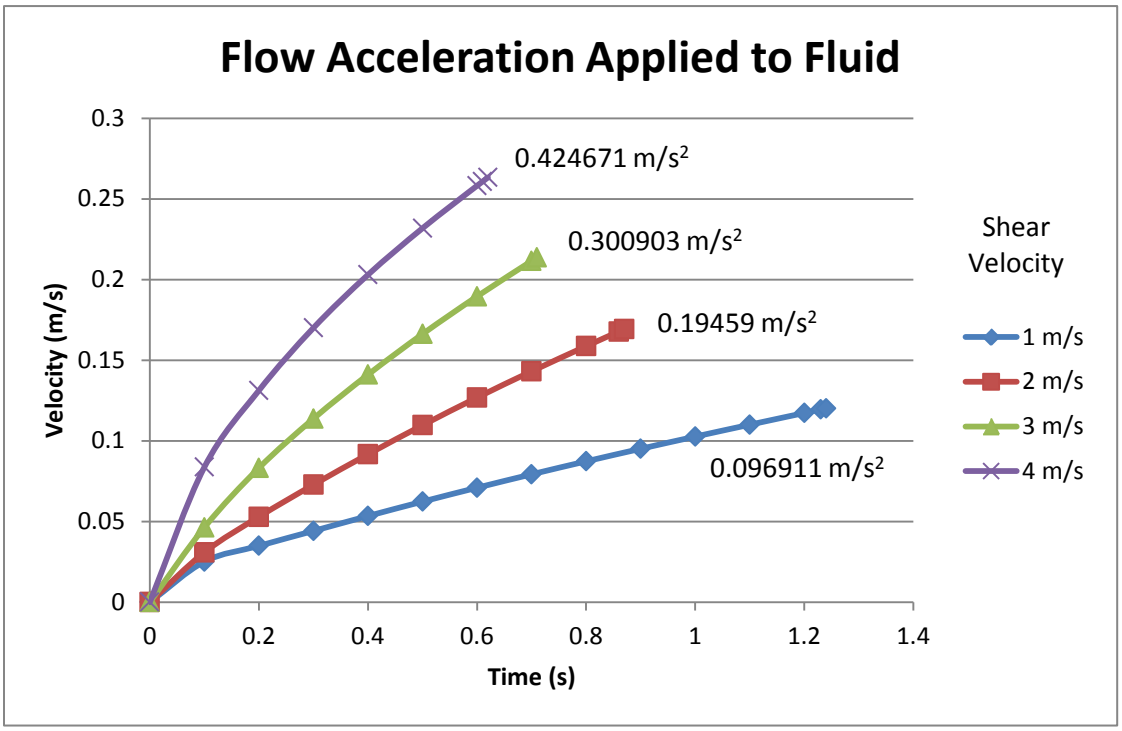

Figure 11. Flow Acceleration Applied to Fluid

The shear stress versus shear strain rate relationship curve was used to compare the STF behavior of the fluid model under the four different flow accelerations applied, and the results were presented in Figure 12 to be compared with the expected relationship as highlighted earlier in the report in Figure 1. It could be seen that the model showed a stronger shear thickening behavior for a higher flow acceleration because the higher acceleration curve has a greater change in the slope (i.e. higher viscosity) as the shear strain rate increases.

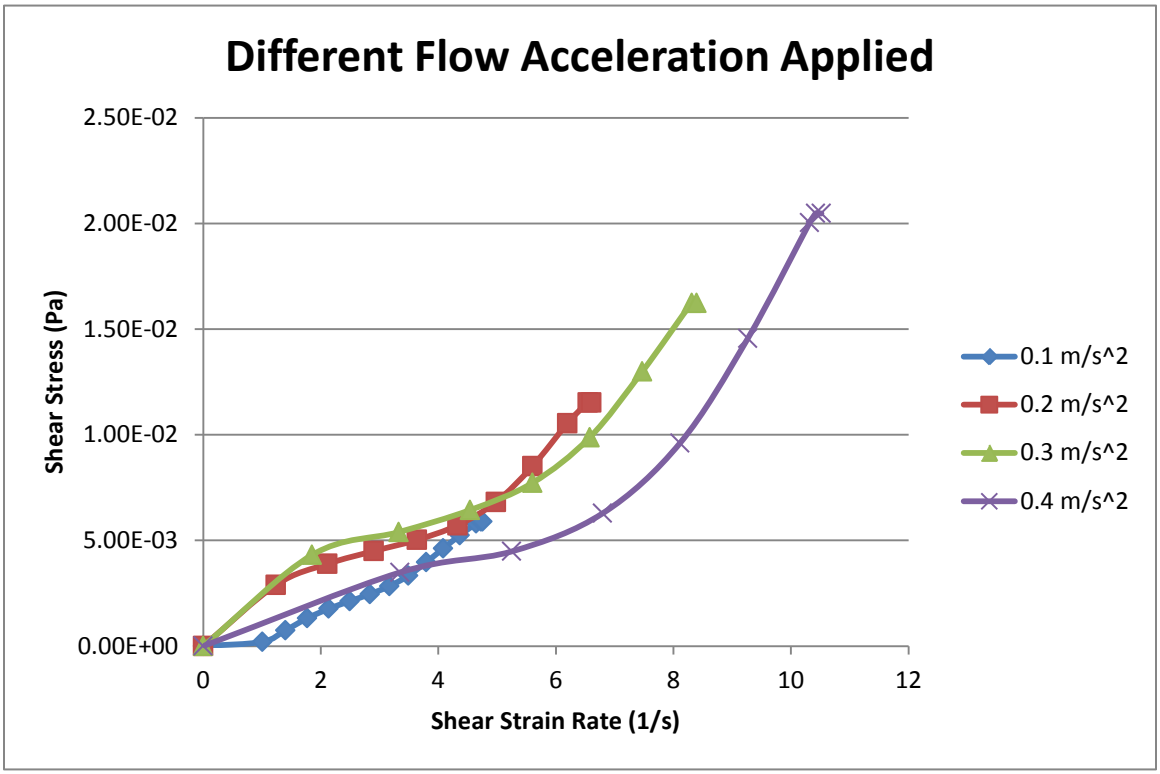

Figure 12. Different Flow Acceleration Applied

The shear thickening effect could also be observed from the apparent-viscosity and shear stress curve in Figure 13. As the concept of viscosity to characterize the shear properties of a fluid could be inadequate to describe non-Newtonian fluids, an apparent or effective viscosity would be defined as a function of shear stress at a particular time. The apparent viscosity was

calculated based on the gradient of the shear stress and shear strain rate at each shear stress value, which was sampled at every 0.1s time step.

The shear thickening effect could be observed in Figure 13, especially beyond the 0.005 Pa regions, where the shear force induced by the applied velocity had reached the top layer of particles shown in Figure 14. Beyond 0.005 Pa, the graph in Figure 13 showed a consistent increase in viscosity as a higher shear stress was experienced. The overall viscosity with the 15 particles embedded in the fluid control volume also showed a higher viscosity as compared to the Newtonian fluid base without particles as shown in the Figure 13.

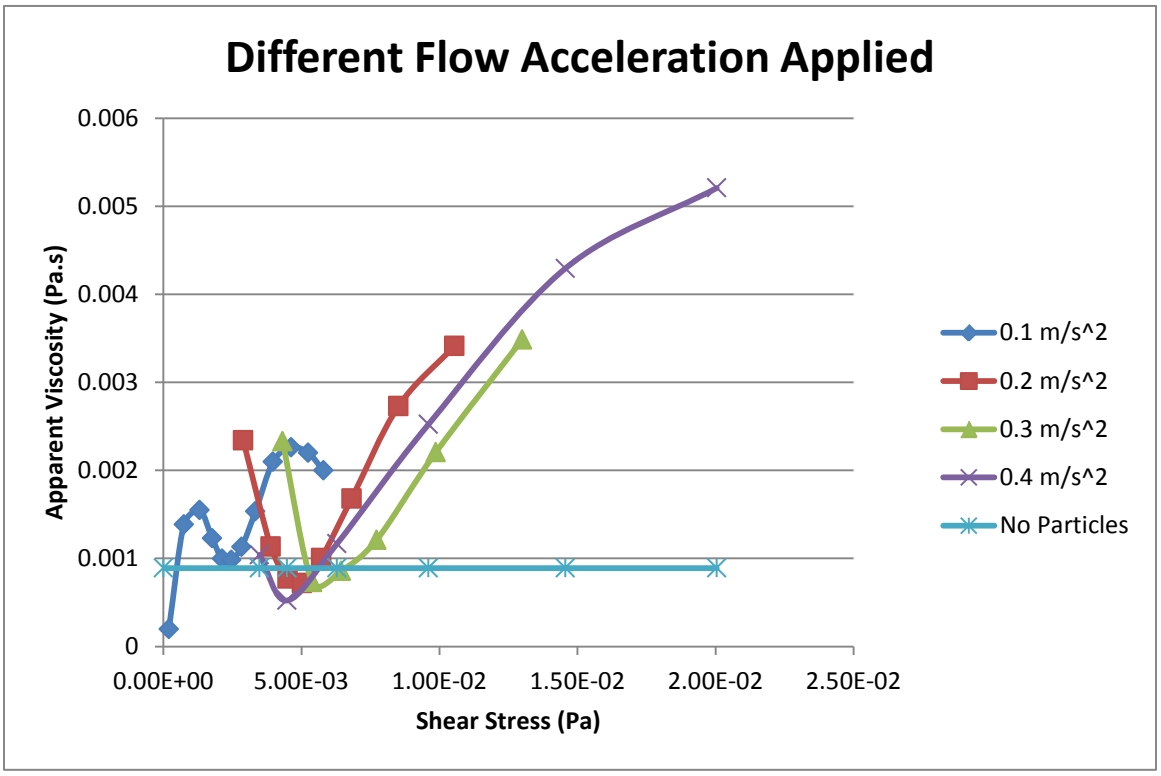

Figure 13. Flow Consistency Index / Viscosity and Shear Stress Curve

At a lower shear stress and shear strain rate (below shear stress of 0.005 Pa and shear strain rate of 2 s^{-1}), the fluid was observed to behave like a Shear Thinning Fluid where the viscosity decreased with higher shear stress. This was likely due to the effect of the shear force travelling along the top slice of the

Newtonian fluid domain and yet to reach the top layer of particles in the STF model. Figures 14 and 15, show the transition when the shear force interact with the top most layer of particles, resulting in an increase in viscosity when the shear stress was increased. In Figure 14, at a time step of 0.1s with a shear strain rate of

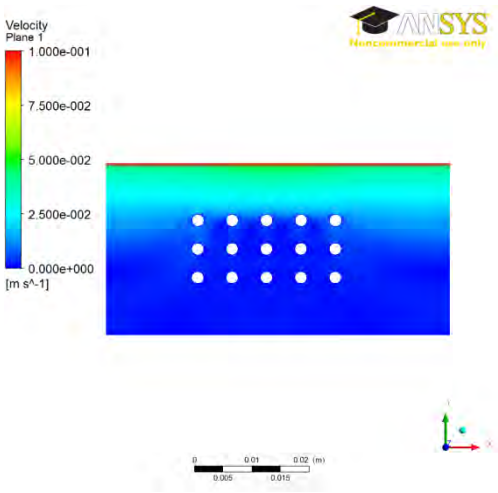

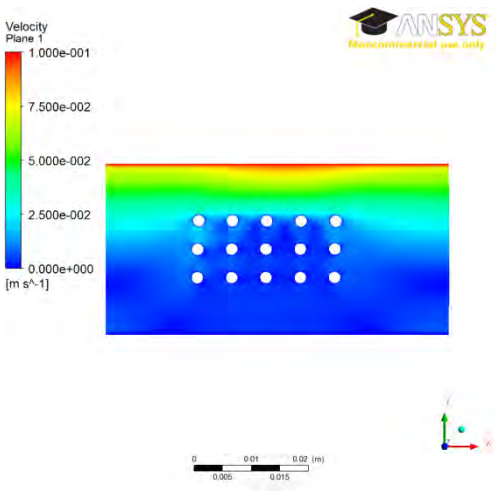

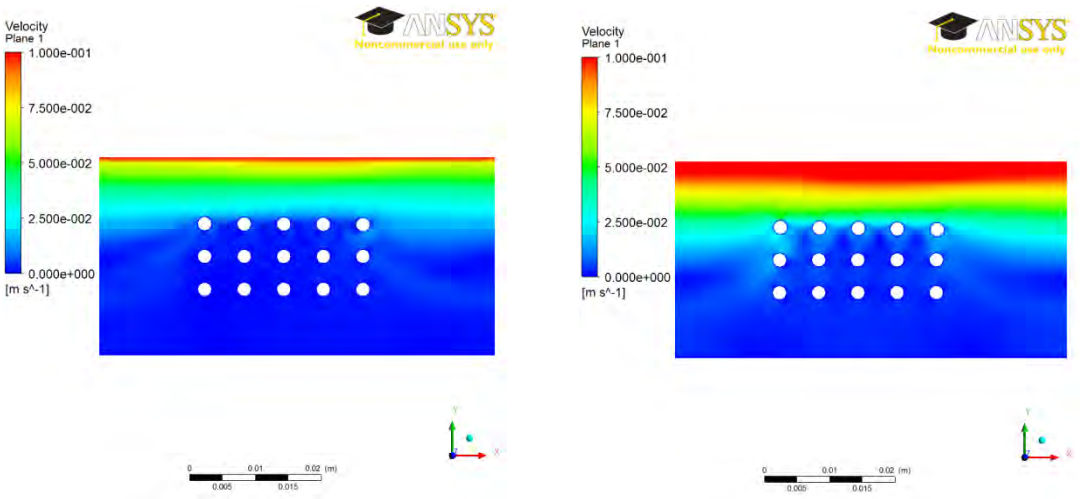

Figure 15. Velocity Profile for Applied Flow Acceleration of 0.4 m/s^2 at 0.1s (left) where

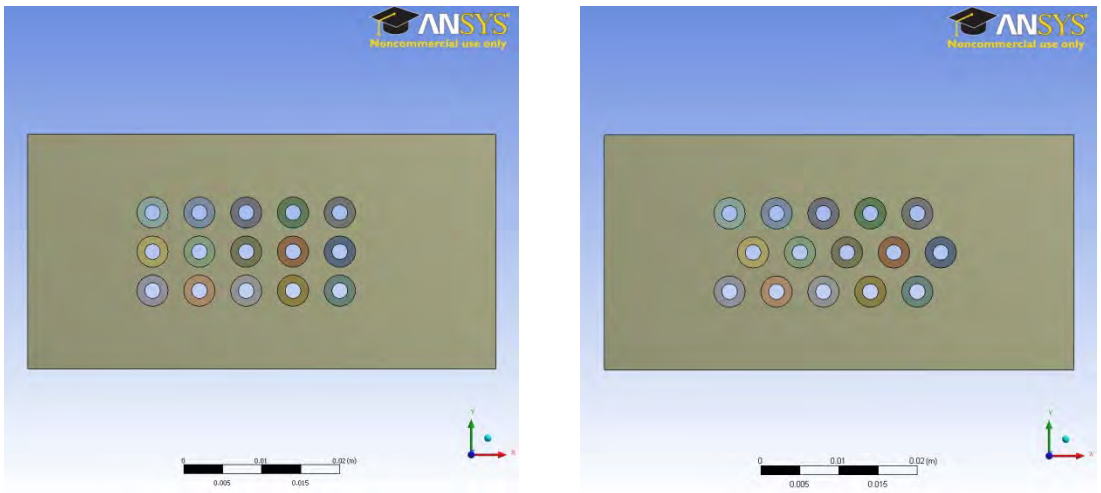

The results was presented in Figure 17. Similar to results in Section A of this chapter, results showed a greater shear thickening effect was observed when a higher flow acceleration was applied for both the uniform or staggered configurations.

It could also be seen from Figure 17 that the uniformly arranged particles showed greater shear thickening, especially at low shear strain rates. The effect of particle arrangement was much less obvious at a lower flow acceleration applied of 0.3 m/s^2 compared to 0.4 m/s^2. This was probably due to the smaller shear force exerted on the particles, and correspondingly slower rate of reaction from the particles in the top layer and thus, aligning themselves to the second layer before the shear force could cause a displacement in the second layer of particles.

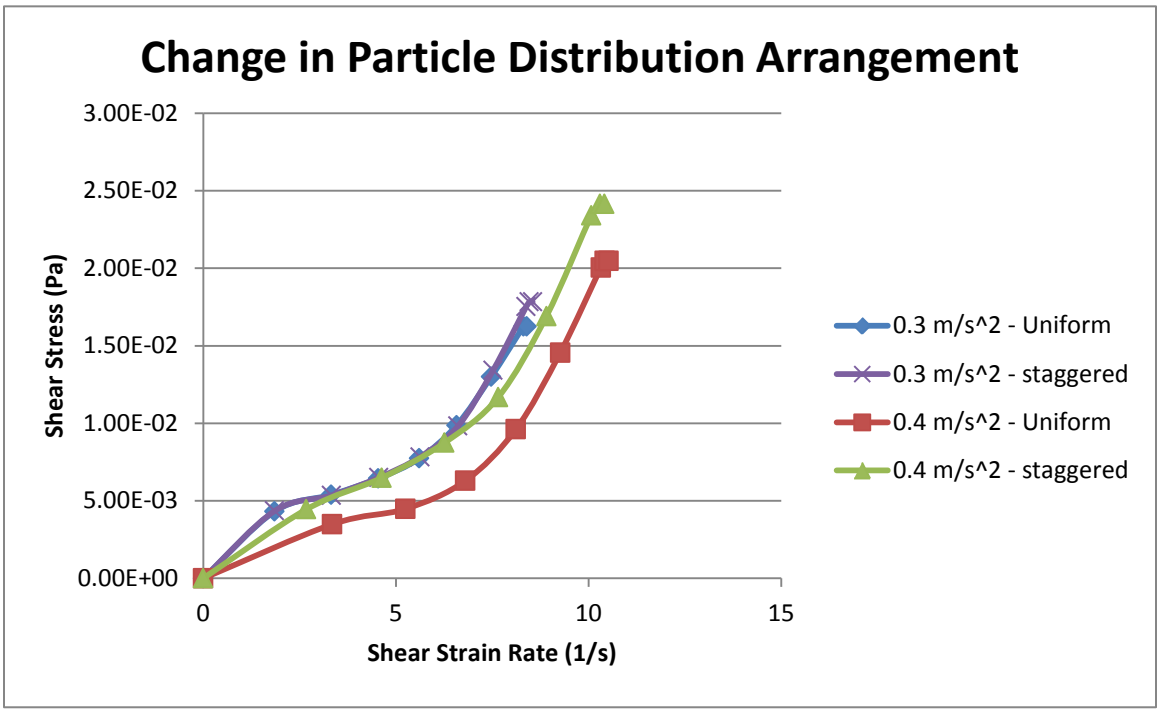

Figure 17. Change in Particle Distribution Arrangement

It could also be observed from the transient velocity plot for a flow acceleration of 0.3m/s^2 in Figure 18 taken at the 0.7s time step for both the uniform and staggered particle arrangements, that the particles would align

themselves in a diagonal pattern, with the top layer in a forward position relative to the direction of the applied shear velocity and the bottom layer trailing behind. It was true for the cases for a flow acceleration of 0.4 m/s^2 as shown in Figure 19.

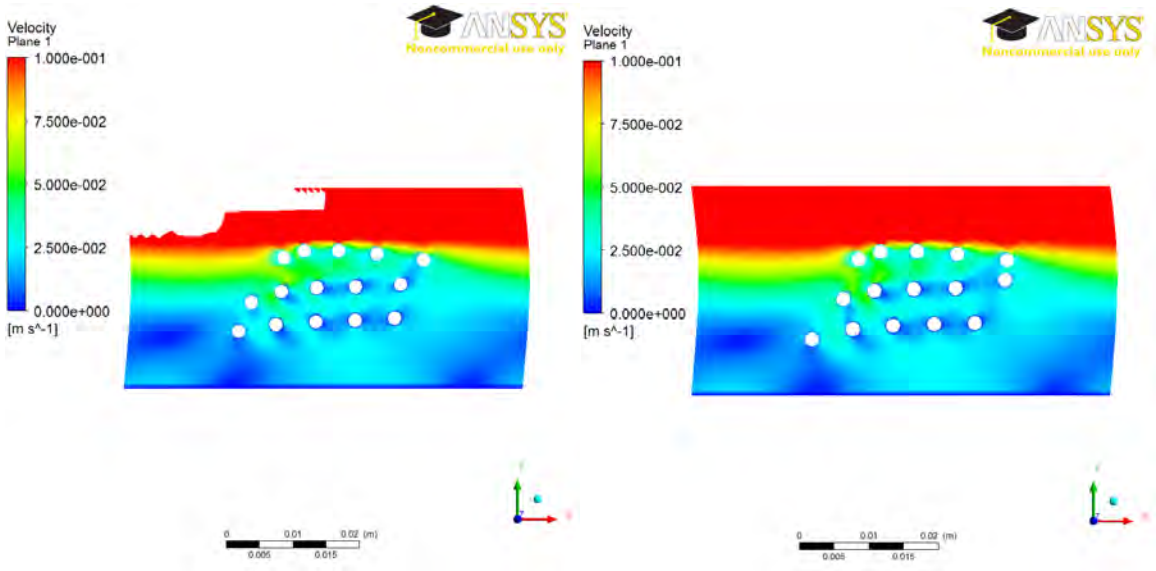

Figure 18. Transient Velocity Plot at 0.7s for Uniform (Left) and Staggered (Right) Particle Distribution for Flow Acceleration of 0.3 m/s^2

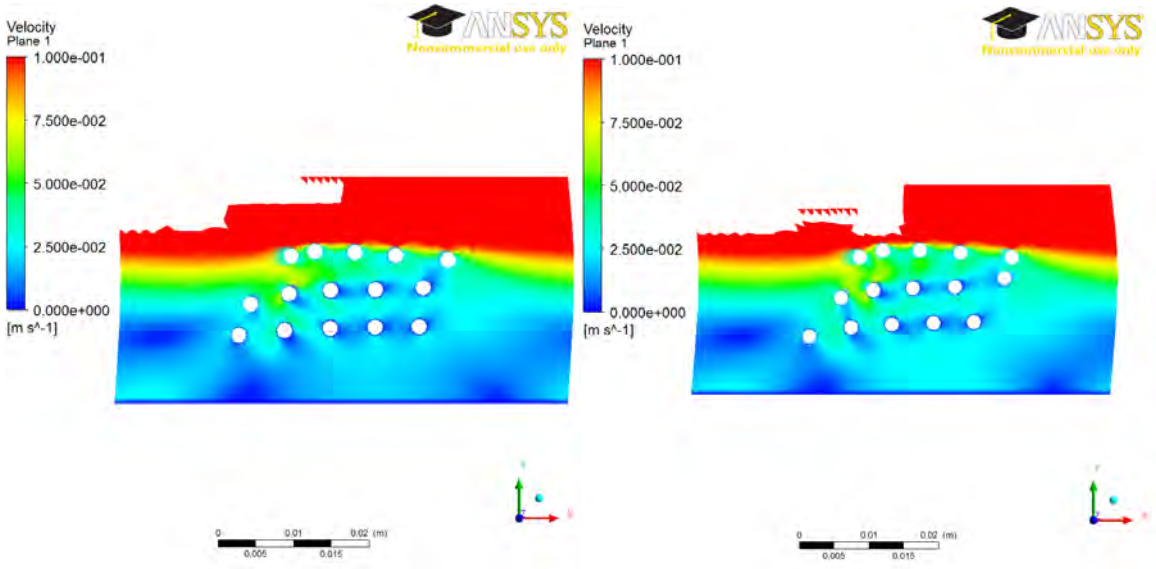

Figure 19. Transient Velocity Plot at 0.6s for Uniform (Left) and Staggered (Right) Particle Distribution for Flow Acceleration of 4 m/s^2

C. FLUID-PARTICLE VOLUME CONCENTRATION

The shear thickening effect affected by the volume concentration of the number of particles in the fluid domain was also investigated. More particles were added to the original model of 15 particles to study the changes in the shear thickening effect at a different flow acceleration applied. Instead of a 3 by 5 particle arrangement, the number of particles was increased to a 3 by 7 configuration of 21 particles, as shown in Figure 20.

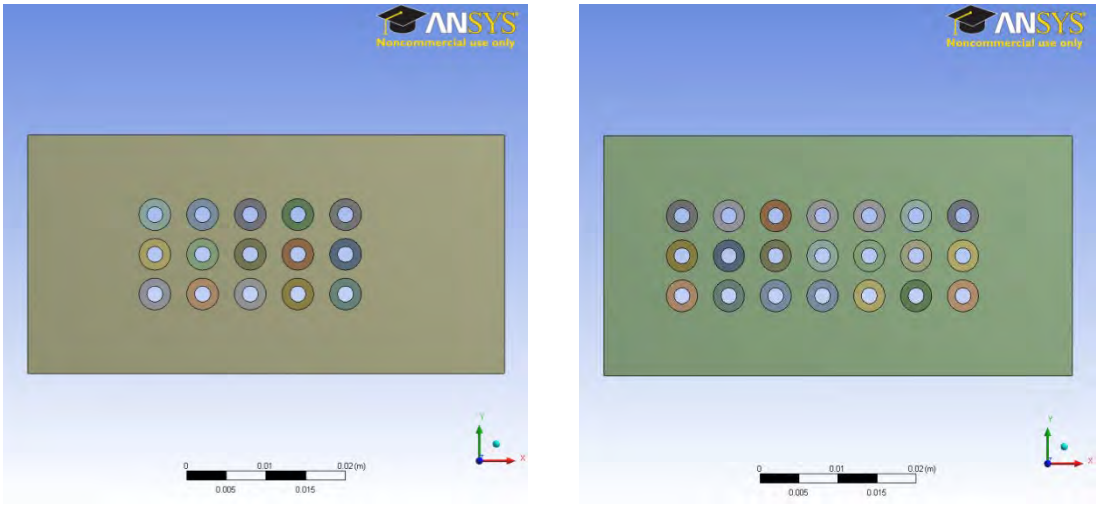

Figure 20. Increase in Number of Particles (Right)

The results, seen in Figure 21, suggested that with a higher number of particles in the fluid, a stronger shear thickening effect was observed, showing lower shear stress level at higher shear strain rate. However, due to the high distortion of the mesh elements resulting in the truncation of the modeling, further data was unobtainable for the models with more particles inserted for higher shear strain rate, although an increasing trend could be observed for shear strain rate beyond 8 s^{-1}.

However, the observation was consistent with empirical studies (Xu et al., 2010; Lee, Wetzel & Wagner, 2003) that compared the shear thickening effect for fluids with different volume concentration of particles. In Xu's study which had experimented with different concentration of shear thickening fluid, it was

observed that energy dissipation was greater with a larger concentration of particles in the STF. The expected shear stress and shear strain rate curve for the results beyond a shear strain rate of 8 s^{-1} was also plotted in Figure 21.

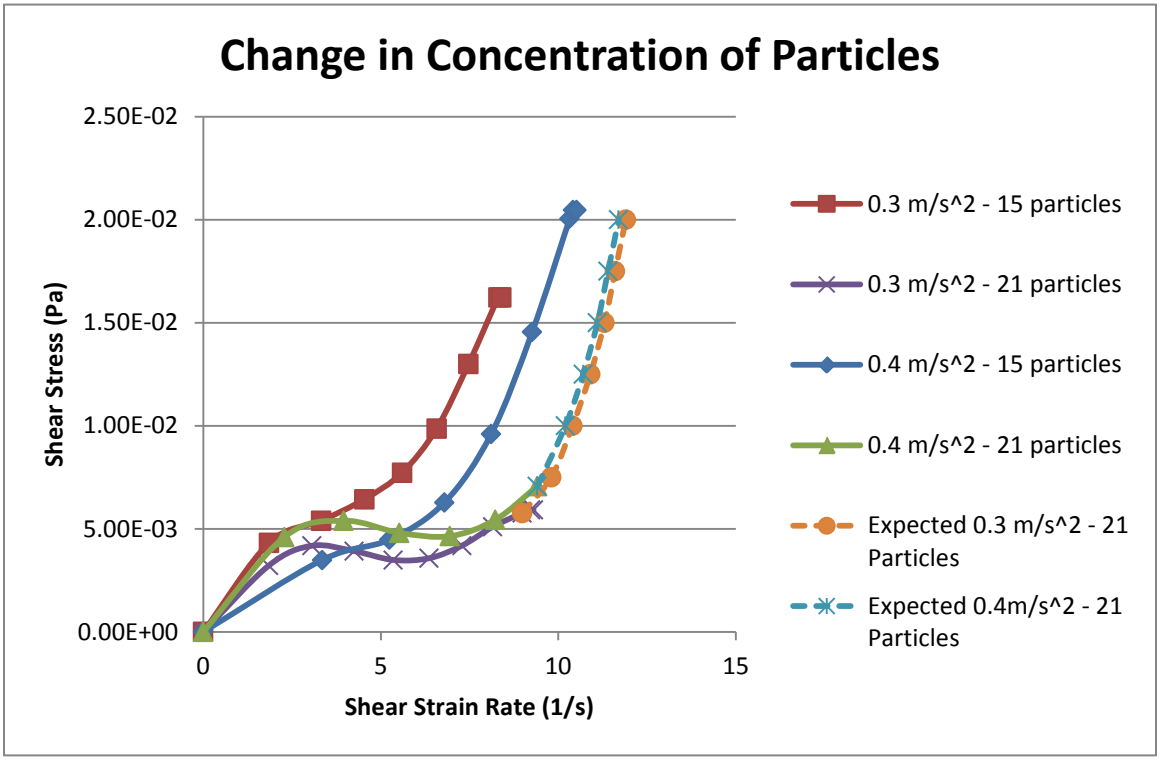

Figure 21. Change in Concentration of Particles

D. PARTICLE SIZE

Two particle sizes were studied to observe its effect on the Shear Thickening Fluid as shown in Figure 22. In the first configuration, 10 2mm diameter particles were used. For the second configuration, the particle size was reduced to 1mm diameter, but the number of particles was increased to 40 particles to keep the total wetted area constant.

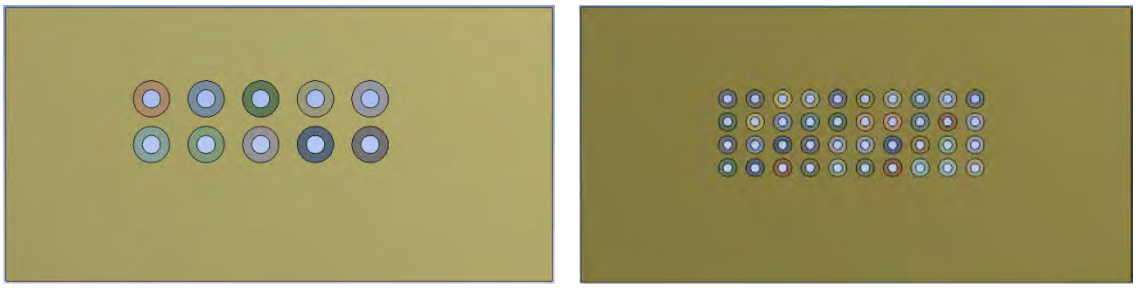

Figure 22. Particle Size – 2mm Diameter Particles (Left) and 1mm Diameter Particles (Right)

The results that could be seen from Figure 23 suggested that the fluid with the smaller diameter particles had a stronger shear thickening effect at lower shear stress levels compared to the larger particles. Unfortunately, the simulation was truncated beyond 4 s^{-1} and the results for the higher shear stress levels could not be determined. This could probably be due to the larger mesh displacement experienced by the smaller particles, when they were subjected to the same flow acceleration. However, the results was consistent with past empirical studies (Lee, Kim & Kim, 2009) on the shear thickening effect due to particle size. In that particular study, it was shown that the silica colloidal suspension using smaller particles yielded a better ballistic performance compared to that of larger particles. The expected behavior of the shear thickening effects beyond the shear strain rate of 4 s^{-1} was also plotted in Figure 23.

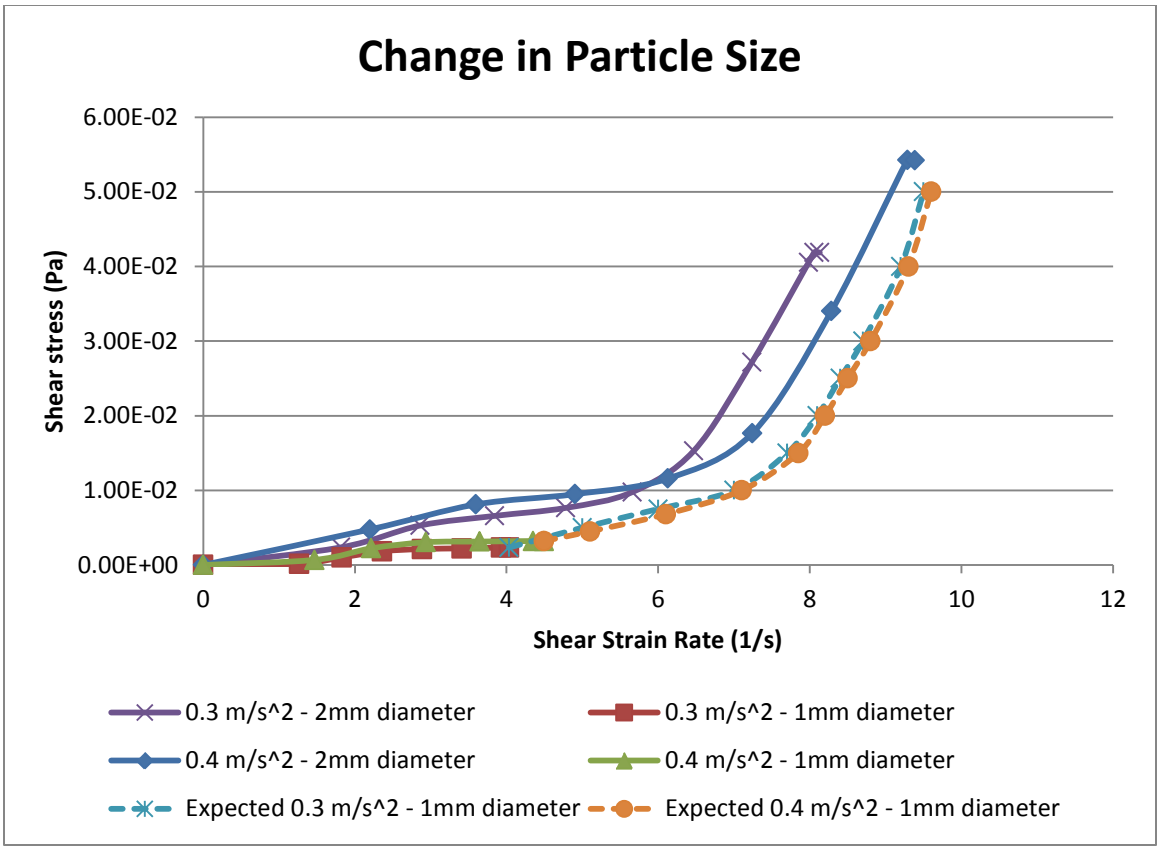

Figure 23. Change in Particle Size

E. PARTICLE SHAPE

The behavior of the Shear Thickening Fluid affected by the shape of particles in the fluid base was also studied. Elliptically shaped particles as shown in Figure 24 were used instead of circular particles, to study the effect of particle shape on shear thickening effect. The presented area and weight of the circular and elliptic particle was kept the same to allow observation in changes in results based purely on the effects of particle shape. The particles were also arranged in two different alignments to study the effect of the shear flow on the longitudinal or lateral ends of the elliptic particles.

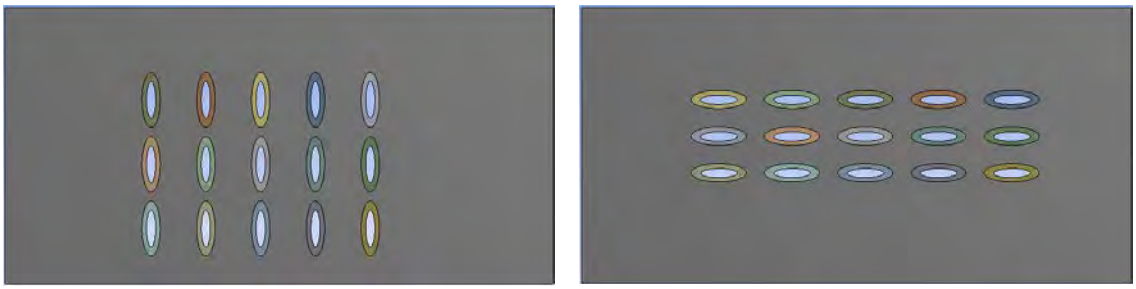

Figure 24. Elliptically-Shaped Particles Arranged in Two Configurations – Vertical (Left) and Horizontal (right)

The results for vertically and horizontally arranged elliptic particles, as well as circular particles in a fluid base subjected to a flow acceleration of 0.3 m/s^2 were summarized in Figure 25. It could be seen from Figure 25 that the elliptical particles generally had lower viscosity at low shear stress and shear strain rate, but significantly higher viscosity at high shear strain regions. This showed that by changing the aspect ratios of the particles dimensions, the shear thickening effect could be improved with the same number of particles.

Due to the early truncation of the simulation with the vertically arranged elliptical particles, the study could only conclude that the fluid had a higher viscosity at lower shear strain rate levels of up to 6 s^{-1} compared to horizontally arranged elliptic particles.

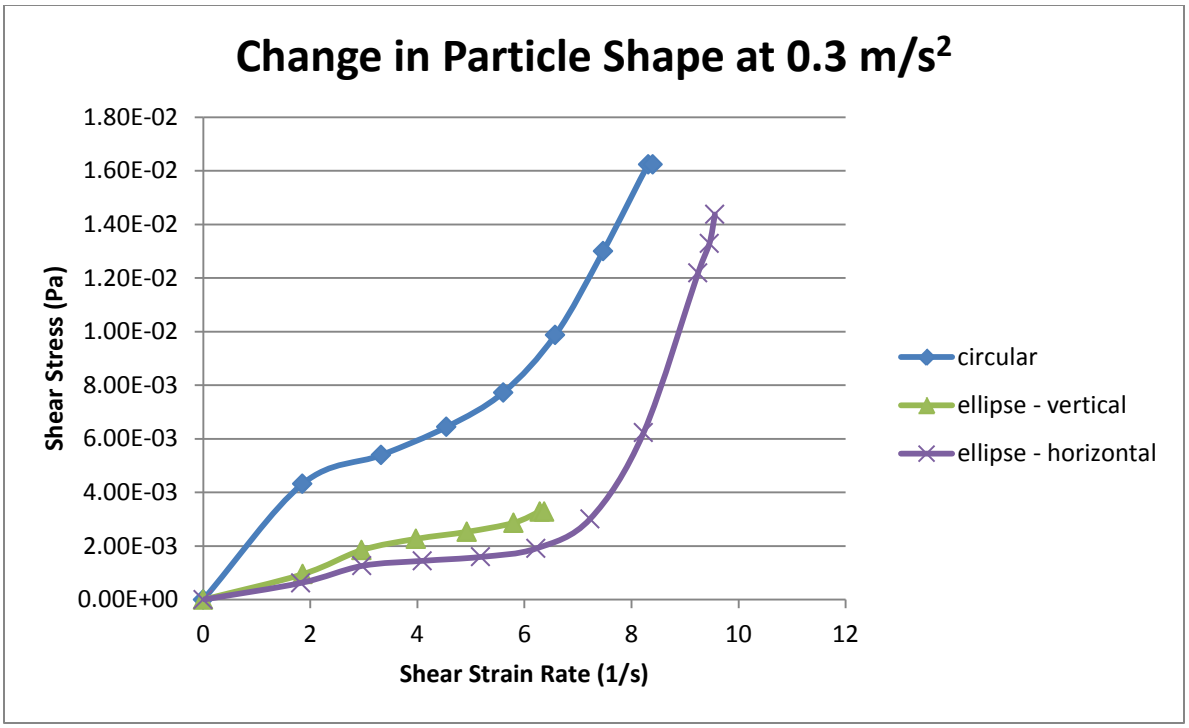

Figure 25. Change in Particle Shape at Flow Acceleration of 0.3 m/s^2

F. NON-NEWTONIAN FLUID BASE

The model was used to study the behavior of particles and their effect on Non-Newtonian Fluids, as compared to Newtonian fluids. The Non-Newtonian fluid used had a viscosity consistency of 1.63 x 10^{-5} Pa.s, and using the Ostwald de Waele model, a power law index of 1.5 was assigned.

Flow acceleration of 0.3 m/s^2 and 0.4 m/s^2 were applied to the non-Newtonian fluid, with the baseline 3 by 5 particle configuration. From the results shown in Figure 26, it was observed that a non-linear response occurred in the lower strain rate and shear stress levels before continuing its increasing trend in shear stress and viscosity above 100 s^{-1}. The expected performance of the NNF without any particles added was also plotted in the graph in Figure 26 for comparison.

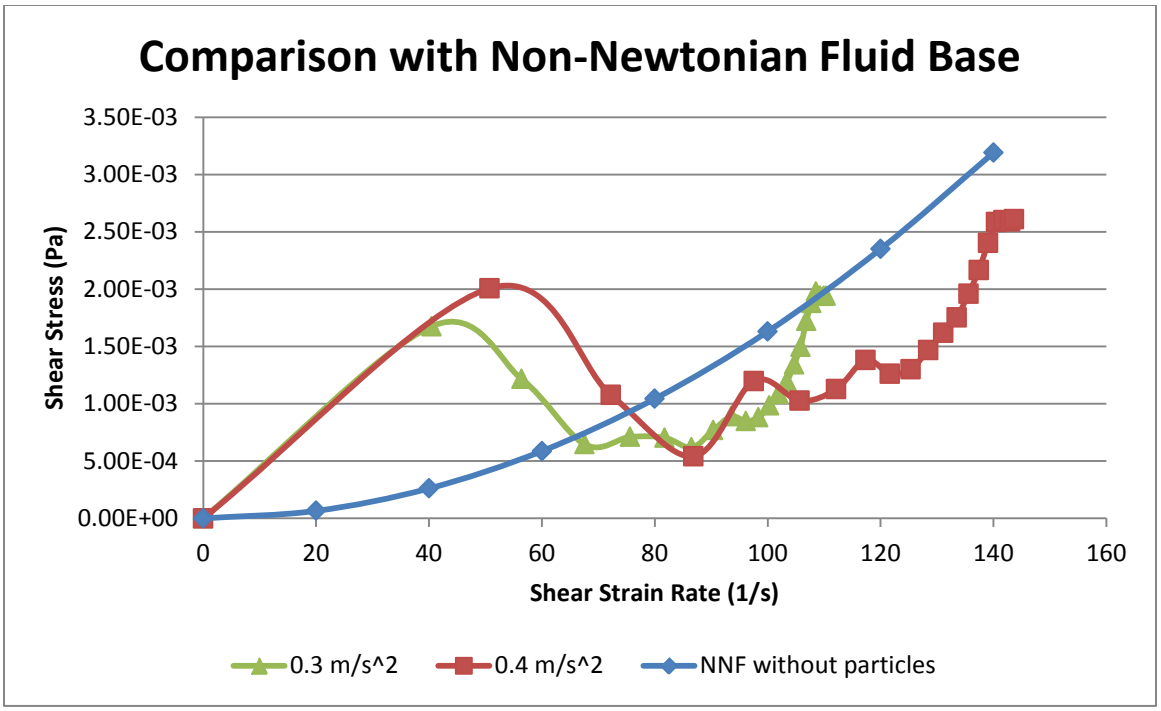

Figure 26. Non-Newtonian Fluid Base

G. SUMMARY OF RESULTS

In summary, the follow parameters were examined to study their shear thickening effects on the STF:

- Applied Flow Acceleration
- Particle Distribution Arrangement
- Volume Concentration of Particles
- Particle Size
- Particle Shape
- Particles in both Newtonian and Non-Newtonian Fluid

The study on the applied flow acceleration showed that the model with the boundaries conditions used was able to simulate the shear thickening effect of the STF. The higher was the applied flow acceleration, the larger was the shear thickening effect. These characteristics showed the potential for the application of the STF against loadings with high shear effects, such as the pressure blast

wave, while maintaining the flexibility of the material in low shear forces, during transportation or at-rest phase.

The study on the distribution of the particles within the fluid base showed that the position of the particles should be as much perpendicular to the expected shear force loading as possible to break up the shear forces exerted on the fluid body. By staggering the particles, the effect on the second layer to resist the shear force was reduced. However, more needs to be studied if the observation was still true if more layers of the particles were modeled, and when the staggered or uniform arrangements were placed more compactly together.

The model suggested that a higher volume concentration of particles contributed to a better shear thickening effect. However, a high concentration of particles could mean an increase in rigidity and weight of the STF. Thus, a trade off study would have to be done to obtain the maximum blast mitigation effect required with the lowest particle concentration.

The model also suggested that a smaller particle size contributed to better mitigation of shear stress applied at low shear stress regions. Further modeling would be required to study if a combination of particle sizes could allow the shear thickening effect to be smoothed out in the transition from the low to high shear stress regions, resulting in less stress on the protective structure itself.

The study on the shape of the particles showed that the aspect ratio of particles played an important role in shear thickening performance. By aligning the particles with higher surface area in the direction of the shear force, a better shear thickening effect could be achieved. This could also translate to savings in the number or volume concentration of particles with a higher aspect ratio required in a STF for the same shear thickening effect.

The results for the study of particles in Non-Newtonian Fluid, which showed a non-linear response at low shear stress levels, could be due to particles interacting with the Eulerian description of the shear thickening fluid used in the study.

The non-linear response could be due to the alignment of particles in the initial stage of flow accelerations before collectively showing an increasing trend of shear thickening effect at a higher shear strain rate.

IV. CONCLUSIONS AND RECOMMENDATIONS

A. CONCLUSION

The numerical analysis on shear thickening was conducted modeling shear-thickening effects due to the fluid base and particle interactions. It allowed the study of key particle parameters that could affect the performance of the STF for blast mitigation applications. This offered an added dimension to the Eulerian methods, as well as empirical approaches used so far.

In summary, the following parameters potentially provided greater shear thickening effect to be achieved:

- Employing the Shear Thickening Fluid for high flow acceleration applications.
- Aligning particle layers perpendicularly to the expected shear force loading.
- Employing a higher concentration of particles possible, with trade-off on weight and flexibility of the material.
- Using a smaller particle size to improve the wetted surface area available, given a constant total volume and weight of the particles used.
- Using particles with high aspect ratios and with the longer surface aligning perpendicular to the expected shear flow.
- Study suggested that particles could be added to further improve the shear thickening effect of Non-Newtonian Fluids, although more have to be investigated on the non-linear response to flow acceleration at low shear stress levels.

Successful numerical analysis of the shear thickening effect would allow more optimized and improved STF for application to blast mitigation materials such as explosive blankets and protective barriers, in addition to the ballistic applications used today.

B. RECOMMENDATIONS

An issue to consider when employing the Shear Thickening Fluid for practical use would be to create an effective energy-absorbing composite to hold

the Shear Thickening Fluid in place. The interaction between the fluid and the envelopment geometry could affect the rheological response of the STFs when subjected to loading (Bettin, 2005). In Bettin's empirical study, the open cell elastomeric foam was used to contain the STF. For this study, a generic rectangular control volume was created to study the effects of the STF alone, without the interference of the container that would be required to hold the fluid together for practical applications.

To improve the modeling capabilities of the current model, it would be recommended to incorporate the ANSYS ICEM meshing software to the CFX processor. The ANSYS ICEM CFD meshing software uses advanced CAD/geometry readers and repair tools to allow the user to model simulations which require higher meshing demand where mesh displacements within the model result in highly skewed elements, thus requiring automatic re-meshing and re-creating models within a simulation processing.

To improve the fidelity of the modeling, a 3-Dimensional model could also be simulated instead of the current 2-D simulation. This would allow particle interactions in the z-direction to be defined. However, this would likely require exponentially more computational time and resources.

APPENDIX A. NUMERICAL DATA FROM MODELING

Flow Acceleration Applied of 0.1 m/s^2

Time (s)	Shear Stress (N/m^2)	Force (N)	Area (m^2)		Viscosity		Utop	Ubottom	du	dy	du/dy
0	0.00E+00	0.00E+00	0.00003				0	0	0	0.025	0
0.1	1.99E-04	5.97E-09	0.00003		1.98E-04		0.025119	9.27E-07	0.02511807	0.025	1.00472292
0.2	7.40E-04	2.22E-08	0.00003		5.30E-04		0.0349007	5.55E-06	0.03489515	0.025	1.39580593
0.3	1.31E-03	3.94E-08	0.00003		7.44E-04		0.0441668	1.71E-05	0.04414971	0.025	1.76598826
0.4	1.77E-03	5.30E-08	0.00003		8.28E-04		0.0534093	3.60E-05	0.05337325	0.025	2.13493016
0.5	2.12E-03	6.37E-08	0.00003		8.52E-04		0.0623458	6.15E-05	0.06228431	0.025	2.49137242
0.6	2.46E-03	7.38E-08	0.00003		8.68E-04		0.0709551	8.71E-05	0.07086804	0.025	2.83472174
0.7	2.83E-03	8.50E-08	0.00003		8.95E-04		0.0792715	0.000125403	0.0791461	0.025	3.16584388
0.8	3.33E-03	1.00E-07	0.00003		9.55E-04		0.0873145	1.98E-05	0.08729466	0.025	3.49178648
0.9	3.97E-03	1.19E-07	0.00003		1.05E-03		0.0950976	0.00022572	0.09487188	0.025	3.7948752
1	4.62E-03	1.39E-07	0.00003		1.13E-03		0.102652	0.000543182	0.10210882	0.025	4.08435272
1.1	5.24E-03	1.57E-07	0.00003		1.20E-03		0.110027	0.000889785	0.10913722	0.025	4.3654886
1.2	5.79E-03	1.74E-07	0.00003		1.25E-03		0.117282	0.00124271	0.11603929	0.025	4.6415716
1.23	5.90E-03	1.77E-07	0.00003		1.25E-03		0.119448	0.00134748	0.11810052	0.025	4.7240208
1.24	5.90E-03	1.77E-07	0.00003		1.24E-03		0.12017	0.0013823	0.1187877	0.025	4.751508

Table 1. Flow Acceleration Applied of 0.1 m/s^2

Flow Acceleration Applied of 0.2 m/s^2

Time (s)	Shear Stress (N/m^2)	Force (N)	Area (m^2)		Viscosity		Utop	Ubottom	du	dy	du/dy
0	0.00E+00	0.00E+00	0.00003				0	0	0	0.025	0
0.1	2.89E-03	8.67E-08	0.00003		2.34E-03		0.030918	2.07E-05	0.03089735	0.025	1.23589389
0.2	3.89E-03	1.17E-07	0.00003		1.84E-03		0.0529324	8.47E-05	0.05284768	0.025	2.11390712
0.3	4.50E-03	1.35E-07	0.00003		1.55E-03		0.072809	2.19E-04	0.07259017	0.025	2.90360696
0.4	5.02E-03	1.51E-07	0.00003		1.38E-03		0.0916745	8.20E-04	0.09085492	0.025	3.63419696
0.5	5.72E-03	1.72E-07	0.00003		1.32E-03		0.109693	1.55E-03	0.10814492	0.025	4.3257968
0.6	6.82E-03	2.05E-07	0.00003		1.37E-03		0.126836	2.32E-03	0.12452	0.025	4.9808
0.7	8.51E-03	2.55E-07	0.00003		1.52E-03		0.143125	0.00307129	0.14005371	0.025	5.6021484
0.8	1.05E-02	3.16E-07	0.00003		1.70E-03		0.158705	3.79E-03	0.15491533	0.025	6.1966132
0.86	1.15E-02	3.46E-07	0.00003		1.76E-03		0.16779	0.00420024	0.16358976	0.025	6.5435904
0.87	1.15E-02	3.46E-07	0.00003		1.75E-03		0.169293	0.0042676	0.1650254	0.025	6.601016

Table 2. Flow Acceleration Applied of 0.2 m/s^2

Flow Acceleration Applied of 0.3 m/s^2

Time (s)	Shear Stress (N/m^2)	Force (N)	Area (m^2)		Viscosity		Utop	Ubottom	du	dy	du/dy
0	0.00E+00	0.00E+00	0.00003				0	0	0	0.025	0
0.1	4.31E-03	1.29E-07	0.00003		2.33E-03		0.0463472	2.84E-05	0.0463188	0.025	1.85275202
0.2	5.39E-03	1.62E-07	0.00003		1.62E-03		0.0832097	1.19E-04	0.08309023	0.025	3.32360928
0.3	6.44E-03	1.93E-07	0.00003		1.42E-03		0.113757	2.10E-04	0.11354651	0.025	4.54186048
0.4	7.73E-03	2.32E-07	0.00003		1.38E-03		0.141043	9.58E-04	0.14008505	0.025	5.60340192
0.5	9.87E-03	2.96E-07	0.00003		1.50E-03		0.166221	1.85E-03	0.16436797	0.025	6.5747188
0.6	1.30E-02	3.90E-07	0.00003		1.74E-03		0.189555	2.78E-03	0.18677736	0.025	7.4710944
0.7	1.62E-02	4.87E-07	0.00003		1.95E-03		0.211493	0.00367859	0.20781441	0.025	8.3125764
0.71	1.62E-02	4.87E-07	0.00003		1.93E-03		0.213641	3.77E-03	0.20987388	0.025	8.3949552

Table 3. Flow Acceleration Applied of 0.3 m/s^2

Flow Acceleration Applied of 0.3 m/s^2 – Staggered Arrangement

Time (s)	Shear Stress (N/m^2)	Force (N)	Area (m^2)		Viscosity		Utop	Ubottom	du	dy	du/dy
0	0.00E+00	0.00E+00	0.00003				0	0	0	0.025	0
0.1	4.34E-03	1.30E-07	0.00003		2.35E-03		0.0463211	2.94E-05	0.0462917	0.025	1.85166815
0.2	5.35E-03	1.61E-07	0.00003		1.61E-03		0.0833027	1.26E-04	0.08317669	0.025	3.32706748
0.3	6.50E-03	1.95E-07	0.00003		1.43E-03		0.114071	1.85E-04	0.11388615	0.025	4.555446
0.4	7.82E-03	2.35E-07	0.00003		1.39E-03		0.141577	9.00E-04	0.14067714	0.025	5.6270856
0.5	9.82E-03	2.95E-07	0.00003		1.49E-03		0.167026	1.78E-03	0.16524975	0.025	6.60999
0.6	1.34E-02	4.03E-07	0.00003		1.78E-03		0.190739	2.70E-03	0.18803794	0.025	7.5215176
0.7	1.75E-02	5.26E-07	0.00003		2.09E-03		0.213138	0.00362131	0.20951669	0.025	8.3806676
0.71	1.78E-02	5.35E-07	0.00003		2.11E-03		0.215327	0.00371266	0.21161434	0.025	8.4645736
0.72	1.78E-02	5.35E-07	0.00003		2.09E-03		0.217515	3.80E-03	0.21371099	0.025	8.5484396

Table 4. Flow Acceleration Applied of 0.3 m/s^2 – Staggered Arrangement

Flow Acceleration Applied of 0.3 m/s^2 – Higher Particle Volume Concentration

Time (s)	Shear Stress (N/m^2)	Force (N)	Area (m^2)		Viscosity		Utop	Ubottom	du	dy	du/dy
0	0.00E+00	0.00E+00	0.00003				0	0	0	0.025	0
0.1	3.21E-03	9.64E-08	0.00003		1.74E-03		0.0461004	4.62E-06	0.04609578	0.025	1.84383107
0.2	4.18E-03	1.25E-07	0.00003		1.37E-03		0.07656	2.99E-05	0.07653013	0.025	3.06120511
0.3	3.92E-03	1.18E-07	0.00003		9.23E-04		0.106281	6.62E-05	0.10621479	0.025	4.24859173
0.4	3.49E-03	1.05E-07	0.00003		6.52E-04		0.133929	9.96E-05	0.13382941	0.025	5.35317629
0.5	3.58E-03	1.07E-07	0.00003		5.62E-04		0.1593	2.05E-04	0.15909457	0.025	6.36378272
0.6	4.19E-03	1.26E-07	0.00003		5.75E-04		0.182577	3.35E-04	0.18224225	0.025	7.2896898
0.7	5.10E-03	1.53E-07	0.00003		6.26E-04		0.204217	0.000348831	0.20386817	0.025	8.15472676
0.8	5.76E-03	1.73E-07	0.00003		6.42E-04		0.224834	0.00027589	0.22455811	0.025	8.9823244
0.83	5.92E-03	1.77E-07	0.00003		6.41E-04		0.230901	0.000244307	0.23065669	0.025	9.22626772
0.84	5.92E-03	1.78E-07	0.00003		6.36E-04		0.232831	2.34E-04	0.23259738	0.025	9.30389508

Table 5. Flow Acceleration Applied of 0.3 m/s^2 – Higher Particle Volume Concentration

Flow Acceleration Applied of 0.3 m/s^2 – 10 Particles of 2mm Diameter

Time (s)	Shear Stress (N/m^2)	Force (N)	Area (m^2)		Viscosity		Utop	Ubottom	du	dy	du/dy
0	0.00E+00	0.00E+00	0.00003				0	0	0	0.025	0
0.1	2.36E-03	7.08E-08	0.00003		1.30E-03		0.0454032	5.21E-06	0.04539799	0.025	1.81591955
0.2	5.29E-03	1.59E-07	0.00003		1.85E-03		0.0715081	4.11E-05	0.071467	0.025	2.85868012
0.3	6.57E-03	1.97E-07	0.00003		1.71E-03		0.0961627	1.10E-04	0.09605282	0.025	3.84211292
0.4	7.65E-03	2.30E-07	0.00003		1.60E-03		0.119638	9.78E-05	0.11954023	0.025	4.78160909
0.5	9.76E-03	2.93E-07	0.00003		1.73E-03		0.142038	5.95E-04	0.14144305	0.025	5.65772208
0.6	1.53E-02	4.58E-07	0.00003		2.36E-03		0.163371	1.69E-03	0.16168598	0.025	6.4674392
0.7	2.72E-02	8.15E-07	0.00003		3.76E-03		0.183816	0.00289883	0.18091717	0.025	7.2366868
0.8	4.05E-02	1.22E-06	0.00003		5.08E-03		0.203685	0.00410296	0.19958204	0.025	7.9832816
0.81	4.19E-02	1.26E-06	0.00003		5.20E-03		0.205648	0.00421929	0.20142871	0.025	8.0571484
0.82	4.19E-02	1.26E-06	0.00003		5.15E-03		0.207611	4.34E-03	0.20327538	0.025	8.1310152

Table 6. Flow Acceleration Applied of 0.3 m/s^2 – 10 Particles of 2mm Diameter

Flow Acceleration Applied of 0.3 m/s^2 – 40 Particles of 1mm Diameter

Time (s)	Shear Stress (N/m^2)	Force (N)	Area (m^2)		Viscosity		Utop	Ubottom	du	dy	du/dy
0	0.00E+00	0.00E+00	0.00003				0	0	0	0.025	0
0.05	1.57E-04	4.70E-09	0.00003		1.24E-04		0.0315947	2.21E-07	0.03159448	0.025	1.26377917
0.1	1.01E-03	3.03E-08	0.00003		5.54E-04		0.0456141	2.32E-07	0.04561387	0.025	1.82455473
0.15	1.84E-03	5.51E-08	0.00003		7.79E-04		0.0589398	5.69E-06	0.05893411	0.025	2.35736422
0.2	2.14E-03	6.41E-08	0.00003		7.41E-04		0.0721646	1.88E-05	0.07214579	0.025	2.8858314
0.25	2.22E-03	6.67E-08	0.00003		6.52E-04		0.0852245	3.98E-05	0.08518468	0.025	3.40738712
0.3	2.33E-03	6.99E-08	0.00003		5.93E-04		0.0982581	6.80E-05	0.09819015	0.025	3.92760582
0.31	2.33E-03	6.98E-08	0.00003		5.77E-04		0.100872	7.43E-05	0.1007977	0.025	4.03190812

Table 7. Flow Acceleration Applied of 0.3 m/s^2 – 40 Particles of 1mm Diameter

Flow Acceleration Applied of 0.3 m/s^2 – Horizontally-Arranged Elliptic Particles

Time (s)	Shear Stress (N/m^2)	Force (N)	Area (m^2)		Viscosity		Utop	Ubottom	du	dy	du/dy
0	0.00E+00	0.00E+00	0.00003		0.00E+00		0	0	0	0.025	0
0.1	6.24E-04	1.87E-08	0.00003		3.42E-04		0.0456137	3.25E-05	0.04558118	0.025	1.82324712
0.2	1.26E-03	3.78E-08	0.00003		4.24E-04		0.0742005	7.64E-05	0.07412415	0.025	2.96496595
0.3	1.45E-03	4.34E-08	0.00003		3.53E-04		0.10247	7.64E-05	0.10239365	0.025	4.09574595
0.4	1.59E-03	4.78E-08	0.00003		3.07E-04		0.129601	1.36E-04	0.12946483	0.025	5.1785932
0.5	1.91E-03	5.72E-08	0.00003		3.07E-04		0.155622	2.47E-04	0.15537515	0.025	6.21500592
0.6	3.01E-03	9.03E-08	0.00003		4.17E-04		0.180803	1.48E-04	0.18065513	0.025	7.22620532
0.7	6.23E-03	1.87E-07	0.00003		7.58E-04		0.20576	1.14E-04	0.20564561	0.025	8.22582448
0.8	1.22E-02	3.66E-07	0.00003		1.32E-03		0.231538	4.60E-04	0.23107754	0.025	9.24310148
0.82	1.33E-02	3.98E-07	0.00003		1.40E-03		0.236919	5.35E-04	0.23638416	0.025	9.45536648
0.83	1.44E-02	4.31E-07	0.00003		1.50E-03		0.239512	0.00057113	0.23894087	0.025	9.55763472

Table 8. Flow Acceleration Applied of 0.3 m/s^2 – Horizontally-Arranged Elliptic Particles

Flow Acceleration Applied of 0.3 m/s^2 – Vertically-Arranged Elliptic Particles

Time (s)	Shear Stress (N/m^2)	Force (N)	Area (m^2)		Viscosity		Utop	Ubottom	du	dy	du/dy
0	0.00E+00	0.00E+00	0.00003		0.00E+00		0	0	0	0.025	0
0.1	9.50E-04	2.85E-08	0.00003		5.11E-04		0.0465279	2.63E-05	0.04650163	0.025	1.86006513
0.2	1.85E-03	5.54E-08	0.00003		6.24E-04		0.0741289	1.44E-04	0.07398539	0.025	2.95941556
0.3	2.27E-03	6.80E-08	0.00003		5.70E-04		0.099669	3.09E-04	0.09936043	0.025	3.97441704
0.4	2.53E-03	7.58E-08	0.00003		5.13E-04		0.123524	4.40E-04	0.12308385	0.025	4.92335408
0.5	2.86E-03	8.59E-08	0.00003		4.94E-04		0.145783	8.83E-04	0.14490049	0.025	5.79601964
0.56	3.29E-03	9.86E-08	0.00003		5.23E-04		0.158428	1.24E-03	0.15718993	0.025	6.2875972
0.57	3.29E-03	9.86E-08	0.00003		5.16E-04		0.160502	0.0012984	0.1592036	0.025	6.368144

Table 9. Flow Acceleration Applied of 0.3 m/s^2 – Vertically-Arranged Elliptic Particles

Flow Acceleration Applied of 0.3 m/s^2 – Non-Newtonian Fluid Base

Time (s)	Shear Stress (N/m^2)	Force (N)	Area (m^2)		Viscosity		Utop	Ubottom	du	dy	du/dy
0	0.00E+00	0.00E+00	0.00003				0	0	0	0.025	0
0.1	1.68E-03	5.03E-08	0.00003		6.51E-06		1.01211	9.13E-07	1.01210909	0.025	40.4843635
0.2	1.22E-03	3.65E-08	0.00003		2.87E-06		1.40951	2.89E-07	1.40950971	0.025	56.3803884
0.3	6.46E-04	1.94E-08	0.00003		1.16E-06		1.68928	6.13E-08	1.68927994	0.025	67.5711975
0.4	7.10E-04	2.13E-08	0.00003		1.08E-06		1.89004	1.36E-07	1.89003986	0.025	75.6015946
0.5	7.03E-04	2.11E-08	0.00003		9.52E-07		2.04362	1.34E-06	2.04361866	0.025	81.7447463
0.6	6.18E-04	1.85E-08	0.00003		7.68E-07		2.16288	0.00E+00	2.16288	0.025	86.5152
0.7	7.70E-04	2.31E-08	0.00003		8.96E-07		2.25876	0.00E+00	2.25876	0.025	90.3504
0.8	8.89E-04	2.67E-08	0.00003		9.83E-07		2.33784	0.00E+00	2.33784	0.025	93.5136
0.9	8.48E-04	2.54E-08	0.00003		9.00E-07		2.40368	0.00E+00	2.40368	0.025	96.1472
1	8.81E-04	2.64E-08	0.00003		9.03E-07		2.45935	0.00E+00	2.45935	0.025	98.374
1.1	9.85E-04	2.96E-08	0.00003		9.81E-07		2.50715	0.00E+00	2.50715	0.025	100.286
1.2	1.09E-03	3.26E-08	0.00003		1.06E-06		2.54865	0.00E+00	2.54865	0.025	101.946
1.3	1.19E-03	3.58E-08	0.00003		1.13E-06		2.58498	0.00E+00	2.58498	0.025	103.3992
1.4	1.34E-03	4.03E-08	0.00003		1.25E-06		2.61703	0.00E+00	2.61703	0.025	104.6812
1.5	1.50E-03	4.49E-08	0.00003		1.38E-06		2.64547	0.00E+00	2.64547	0.025	105.8188
1.6	1.72E-03	5.16E-08	0.00003		1.56E-06		2.67081	0.00E+00	2.67081	0.025	106.8324
1.7	1.88E-03	5.64E-08	0.00003		1.68E-06		2.69342	0.00E+00	2.69342	0.025	107.7368
1.8	1.98E-03	5.94E-08	0.00003		1.75E-06		2.71366	0.00E+00	2.71366	0.025	108.5464
1.9	1.94E-03	5.83E-08	0.00003		1.70E-06		2.73189	0.00E+00	2.73189	0.025	109.2756
2	1.94E-03	5.82E-08	0.00003		1.68E-06		2.74853	0.00E+00	2.74853	0.025	109.9412
2.06	1.94E-03	5.82E-08	0.00003		1.68E-06		2.75792	0.00E+00	2.75792	0.025	110.3168

Table 10. Flow Acceleration Applied of 0.3 m/s^2 – Non-Newtonian Fluid Base

Flow Acceleration Applied of 0.4 m/s^2

Time (s)	Shear Stress (N/m^2)	Force (N)	Area (m^2)		Viscosity		Utop	Ubottom	du	dy	du/dy
0	0.00E+00	0.00E+00	0.00003				0	0	0	0.025	0
0.1	3.49E-03	1.05E-07	0.00003		1.04E-03		0.0837229	2.06E-05	0.08370228	0.025	3.34809101
0.2	4.48E-03	1.34E-07	0.00003		8.53E-04		0.131244	7.72E-05	0.13116676	0.025	5.24667052
0.3	6.28E-03	1.89E-07	0.00003		9.25E-04		0.17004	1.37E-04	0.16990266	0.025	6.79610656
0.4	9.61E-03	2.88E-07	0.00003		1.18E-03		0.202968	1.69E-04	0.20279926	0.025	8.11197028
0.5	1.46E-02	4.37E-07	0.00003		1.57E-03		0.231828	1.96E-04	0.2316323	0.025	9.26529188
0.6	2.00E-02	6.01E-07	0.00003		1.94E-03		0.258179	2.08E-04	0.25797097	0.025	10.3188388
0.61	2.05E-02	6.14E-07	0.00003		1.96E-03		0.260737	0.00026872	0.26046828	0.025	10.4187312
0.62	2.05E-02	6.14E-07	0.00003		1.95E-03		0.263296	3.29E-04	0.26296659	0.025	10.5186636

Table 11. Flow Acceleration Applied of 0.4 m/s^2

Flow Acceleration Applied of 0.4 m/s^2 – Staggered Arrangement

Time (s)	Shear Stress (N/m^2)	Force (N)	Area (m^2)		Viscosity		Utop	Ubottom	du	dy	du/dy
0	0.00E+00	0.00E+00	0.00003				0	0	0	0.025	0
0.1	4.44E-03	1.33E-07	0.00003		1.66E-03		0.0668858	2.92E-05	0.06685657	0.025	2.67426269
0.2	6.48E-03	1.95E-07	0.00003		1.40E-03		0.115962	1.05E-04	0.11585737	0.025	4.63429468
0.3	8.74E-03	2.62E-07	0.00003		1.40E-03		0.156521	4.01E-05	0.15648091	0.025	6.25923621
0.4	1.17E-02	3.50E-07	0.00003		1.53E-03		0.192001	6.40E-04	0.19136133	0.025	7.65445336
0.5	1.69E-02	5.07E-07	0.00003		1.90E-03		0.224292	1.62E-03	0.2226671	0.025	8.906684
0.6	2.34E-02	7.02E-07	0.00003		2.32E-03		0.25452	2.71E-03	0.25181188	0.025	10.0724752
0.62	2.41E-02	7.24E-07	0.00003		2.34E-03		0.260434	0.00292851	0.25750549	0.025	10.3002196
0.62	2.41E-02	7.24E-07	0.00003		2.32E-03		0.263388	3.04E-03	0.26034919	0.025	10.4139676

Table 12. Flow Acceleration Applied of 0.4 m/s^2 – Staggered Arrangement

Flow Acceleration Applied of 0.4 m/s^2 – Higher Particle Volume Concentration

Time (s)	Shear Stress (N/m^2)	Force (N)	Area (m^2)		Viscosity		Utop	Ubottom	du	dy	du/dy
0	0.00E+00	0.00E+00	0.00003				0	0	0	0.025	0
0.1	4.60E-03	1.38E-07	0.00003		2.02E-03		0.0571094	1.11E-05	0.05709828	0.025	2.28393129
0.2	5.39E-03	1.62E-07	0.00003		1.36E-03		0.0989355	5.24E-05	0.09888312	0.025	3.95532481
0.3	4.81E-03	1.44E-07	0.00003		8.70E-04		0.138158	1.01E-04	0.13805705	0.025	5.52228204
0.4	4.64E-03	1.39E-07	0.00003		6.69E-04		0.173888	2.42E-04	0.17364622	0.025	6.94584896
0.5	5.45E-03	1.63E-07	0.00003		6.62E-04		0.206152	4.19E-04	0.20573281	0.025	8.22931252
0.6	7.07E-03	2.12E-07	0.00003		7.51E-04		0.235613	4.26E-04	0.23518719	0.025	9.40748744
0.7	8.19E-03	2.46E-07	0.00003		7.79E-04		0.263308	0.000311772	0.26299623	0.025	10.5198491
0.72	8.29E-03	2.49E-07	0.00003		7.72E-04		0.26872	0.00028102	0.26843898	0.025	10.7375592
0.73	8.29E-03	2.49E-07	0.00003		7.64E-04		0.271422	2.66E-04	0.27115649	0.025	10.8462596

Table 13. Flow Acceleration Applied of 0.4 m/s^2 – Higher Particle Volume Concentration

Flow Acceleration Applied of 0.4 m/s^2 – 10 Particles of 2mm Diameter

Time (s)	Shear Stress (N/m^2)	Force (N)	Area (m^2)		Viscosity		Utop	Ubottom	du	dy	du/dy
0	0.00E+00	0.00E+00	0.00003				0	0	0	0.025	0
0.1	4.76E-03	1.43E-07	0.00003		2.16E-03		0.054941	1.34E-05	0.0549276	0.025	2.19710383
0.2	8.11E-03	2.43E-07	0.00003		2.26E-03		0.0899261	8.25E-05	0.08984363	0.025	3.59374524
0.3	9.49E-03	2.85E-07	0.00003		1.94E-03		0.122766	1.49E-04	0.12261666	0.025	4.90466648
0.4	1.16E-02	3.47E-07	0.00003		1.89E-03		0.153881	7.09E-04	0.15317184	0.025	6.12687376
0.5	1.76E-02	5.29E-07	0.00003		2.44E-03		0.183203	2.19E-03	0.18101032	0.025	7.2404128
0.6	3.40E-02	1.02E-06	0.00003		4.10E-03		0.210932	3.83E-03	0.20709805	0.025	8.283922
0.7	5.43E-02	1.63E-06	0.00003		5.84E-03		0.237601	0.00543337	0.23216763	0.025	9.2867052
0.62	5.42E-02	1.63E-06	0.00003		5.78E-03		0.240232	5.59E-03	0.23464423	0.025	9.3857692

Table 14. Flow Acceleration Applied of 0.4 m/s^2 – 10 Particles of 2mm Diameter

Flow Acceleration Applied of 0.4 m/s^2 – 40 Particles of 1mm Diameter

Time (s)	Shear Stress (N/m^2)	Force (N)	Area (m^2)		Viscosity		Utop	Ubottom	du	dy	du/dy
0	0.00E+00	0.00E+00	0.00003				0	0	0	0.025	0
0.05	6.83E-04	2.05E-08	0.00003		4.65E-04		0.0367263	1.95E-07	0.03672611	0.025	1.46904421
0.1	2.23E-03	6.70E-08	0.00003		1.01E-03		0.055419	4.80E-06	0.0554142	0.025	2.21656796
0.15	3.05E-03	9.14E-08	0.00003		1.04E-03		0.0734844	2.13E-05	0.07346312	0.025	2.93852492
0.2	3.14E-03	9.41E-08	0.00003		8.60E-04		0.0912226	5.08E-05	0.09117178	0.025	3.64687107
0.25	3.21E-03	9.63E-08	0.00003		7.38E-04		0.108876	9.69E-05	0.10877909	0.025	4.35116352
0.26	3.21E-03	9.62E-08	0.00003		7.14E-04		0.112416	1.08E-04	0.1123076	0.025	4.49230416

Table 15. Flow Acceleration Applied of 0.4 m/s^2 – 40 Particles of 1mm Diameter

Flow Acceleration Applied of 0.4 m/s^2 – Non-Newtonian Fluid Base

Time (s)	Shear Stress (N/m^2)	Force (N)	Area (m^2)		Viscosity		Utop	Ubottom	du	dy	du/dy
0	0.00E+00	0.00E+00	0.00003				0	0	0	0.025	0
0.1	2.01E-03	6.02E-08	0.00003		5.55E-06		1.26834	4.29E-07	1.26833957	0.025	50.7335828
0.2	1.08E-03	3.23E-08	0.00003		1.75E-06		1.8057	1.05E-06	1.80569895	0.025	72.2279581
0.3	5.41E-04	1.62E-08	0.00003		6.68E-07		2.17165	1.84E-07	2.17164982	0.025	86.8659926
0.4	1.20E-03	3.60E-08	0.00003		1.24E-06		2.43844	9.32E-07	2.43843907	0.025	97.5375627
0.5	1.03E-03	3.08E-08	0.00003		9.45E-07		2.6414	1.34E-06	2.64139866	0.025	105.655946
0.6	1.13E-03	3.38E-08	0.00003		9.49E-07		2.80269	2.43E-06	2.80268757	0.025	112.107503
0.7	1.38E-03	4.15E-08	0.00003		1.09E-06		2.93317	3.37E-06	2.93316663	0.025	117.326665
0.8	1.26E-03	3.79E-08	0.00003		9.40E-07		3.04145	2.84E-06	3.04144716	0.025	121.657886
0.9	1.30E-03	3.90E-08	0.00003		9.28E-07		3.1329	1.65E-06	3.13289835	0.025	125.315934
1	1.47E-03	4.40E-08	0.00003		1.01E-06		3.211	1.44E-06	3.21099856	0.025	128.439942
1.1	1.62E-03	4.85E-08	0.00003		1.08E-06		3.27846	1.48E-06	3.27845852	0.025	131.138341
1.2	1.75E-03	5.26E-08	0.00003		1.14E-06		3.3374	1.53E-06	3.33739847	0.025	133.495939
1.3	1.96E-03	5.88E-08	0.00003		1.24E-06		3.38934	1.48E-06	3.38933852	0.025	135.573541
1.4	2.17E-03	6.50E-08	0.00003		1.34E-06		3.43534	8.06E-07	3.43533919	0.025	137.413568
1.5	2.40E-03	7.21E-08	0.00003		1.47E-06		3.47619	7.65E-07	3.47618923	0.025	139.047569
1.6	2.59E-03	7.76E-08	0.00003		1.55E-06		3.51251	3.77E-06	3.51250623	0.025	140.500249
1.7	2.60E-03	7.80E-08	0.00003		1.54E-06		3.54493	8.17E-06	3.54492183	0.025	141.796873
1.8	2.59E-03	7.77E-08	0.00003		1.52E-06		3.57416	1.33E-05	3.5741467	0.025	142.965868
1.86	2.61E-03	7.83E-08	0.00003		1.52E-06		3.59052	1.68E-05	3.59050324	0.025	143.620129

Table 16. Flow Acceleration Applied of 0.4 m/s^2 – Non-Newtonian Fluid Base

LIST OF REFERENCES

Anderson, John D. 1995. *Computational Fluid Dynamics: The Basics With Applications.* McGraw-Hill Science.

ANSYS. 2010. *Introduction to ANSYS FLUENT.* Customer Training Material.

ANSYS. 2011. "ANSYS CFD" Accessed September 28, 2011. http://www.ansys.com/Products/Simulation+Technology/Fluid+Dynamics/ANSYS+CFD

Baraff, David. 2001. *Rigid Body Simulation.* Siggraph 2001 Course Notes.

Bettin, Giorgia. 2005. *Energy Absorption of Reticulated Foams Filled with Shear Thickening Silica Suspensions.* Thesis, Massachusetts Institute of Technology.

Boek, E.S., Coveney, P.V., Lekkerkerker, H.N.W., van der Schoot, P.. 1997. *Simulating the Rheology of Dense Colloidal Suspensions Using Dissipative Particle Dynamics.* Physical Review E, Volume 55, Number 3, pp. 3124-3133.

Decker, M.J., Halbach, C.J., Wetzel, E. D., Nam, C.H., Wagner, N.J., Wetzel, E.D.. 2007. *Stab Resistance of Shear Thickening Fluid (STF)-Treated Fabrics.* Science Direct Composite Science and Techonology 67 (2007) 565-578.

EDR, 2011. "CFD Tutorial - Rigid Body Modeling" Accessed October 30 2011. http://www.edr.no/blogg/ansys_bloggen/cfd_tutorial_rigid_body_modeling

Egres Jr, R. G., Lee, Y. S., Kirkwood, J. E., Wetzel, E. D., Wagner, N. J.. 2004. *"Liquid Armor": Protective Fabrics Utilizing Shear Thickening Fluids.* Paper presented at IFAI 4th Int. Conf. on Safety and Protective Fabrics, Pittsburg, PA, 26-27 October, 2004.

Ein-Mozaffari, Farhad, Upreti, Simant R.. 2010. *Investigation of Mixing in Shear Thinning Fluids Using Computational Fluid Dynamics.* In *Computational Fluid Dynamics*, edited by Hyoung Woo Oh, 77-102. InTech . Available from: http://www.intechopen.com/articles/show/title/investigation-of-mixing-in-shear-thinning-fluids-using-computational-fluid-dynamics

Foss, David R., Brady, John F.. 2000. *Structure, Diffusion and Rheology of Brownian Suspensions by Stokesian Dynamics Simulation.* J. Fluid Mech. (2000), vol. 407, pp. 167-200.

Glowinski, R., Pan, T.-W., Hesla, T.I., Joseph, D. D.. 2000. *A Distributed Lagrange Multiplier/Fictitious Domain Method for Particulate Flows.* International Journal of Multiphase Flow, Volume 25, Issue 5, August 1999, pp. 755-794.

Hamaker, H.C.. 1937. *The London-Van der Waals Attraction Between Spherical Particles.* Physics IV No.10.

Jacobs, M. J. N., van Dingenen, J. L. J.. 2001. *Ballistic Protection Mechanisms in Personal Armor.* Journal of Material Science 36 (2001) 3137-3142.

Kambouchev, Nayden. 2007. *Analysis of Blast Mitigation Strategies Exploiting Fluid-Structure Interaction.* Massachusetts Institute of Technology. Published in partial fulfillment in the requirements for the degree of Doctor of Philosophy in Aeronautics and Astronautics.

Ladeinde, Foluso, Nearon, Michelle D.. 1997. *CFD Applications in the HVAC&R Industry.* Massachusetts Institute of Technology. Published in ASHRAE Jornal; Jan 1997; 39, 1; ProQuest Education Journals pg 44.

Lee, Bok-Won, Kim, Il-Jin, Kim, Chun-Gon. 2009. *The Influence of the Particle Size of Silica on the Ballistic Performance of Fabrics Impregnated with Silica Colloidal Suspension.* Journal of Composite Materials, Vil. 43, No. 23/2009.

Lee, Y. S., Gong, Wetzel, E. D., Egres Jr, R. G., Wagner, N. J.. 2002. *Advanced Body Armor Utilizing Shear Thickening Fluids.* 23rd Army Science Conference.

Lee, Young S., Wetzel, E. D., Wagner, N.J.. 2003. *The Ballistic Impact Characteristics of Kevlar Woven Fabrics Impregnated With a Colloidal Shear Thickening Fluid.* Journal of Materials Science 38 (2003) 2825-2833.

Livingston, Ian S. and O'Hanlon, Michael. 2011. *Afghanistan Index - Tracking Variables of Reconstruction and Security in Post-9/11 Afghanistan.* Brookings.

Mernoff, Stephen T., Correia, Stephen. 2010. *Military Blast Injury in Iraq and Afghanistan: The Veterens Health Administration's Polytrauma System of Care.* Medicine & Health/Rhode Island Volume 93 No. 1 January 2010.

Nesterenko, Vitali F.. 2003. *Shock (Blast) Mitigation by 'Soft' Condensed Matter.* CRS Report for Congress. University of California, San Diego. Originally published in MRS Symp. Proc., vol.759.

Petkova, Svetla, Hossain, Alamgir, Naser, Jamal, and Palombo, Enzo. 2003. *CFD Modeling of Blood Flow in Portal Vein Hypertension With and Without Thrombosis.* Paper presented in Third International Conference on CFD in the Minerals and Process Industries CSIRO, Melborne, Australia, 10-12 December 2003.

Solidworks. 2011. *Solidworks Packages.* Accessed 2 November 2011. http://www.solidworks.com/sw/products/10141_ENU_HTML.htm.

Warden D.. 2006. *Military TBI during the Iraq and Afghanistan Wars.* J Head Trauma Rehab 2006; 21:398-402.

Wilson, Clay. 2006. *Improvised Explosive Devices (IEDs) in Iraq and Afghanistan: Effects and Counterasures.* CRS Report for Congress.

Xu, Yu-lei, Gong, Xing-long, Peng, Chao, Sun, Yun-qiang, Jiang, Wan-quan, Zhang, Zhong. 2010. *Shear Thickening Fluids Based on Additives with Different Concentrations and Molecular Chain Lengths.* Chinese Journal of Chemical Physics Volume 23, Number 3.

Zhang Z., Chen Q.. 2006. *Comparison of Eulerian and Lagrangian Methods for Predicting Particle Transport in Enclosed Spaces.* Accepted by Atmospheric Environment in 2006.

THIS PAGE INTENTIONALLY LEFT BLANK

INITIAL DISTRIBUTION LIST

1. Defense Technical Information Center
   Ft. Belvoir, Virginia

2. Dudley Knox Library
   Naval Postgraduate School
   Monterey, California

3. Young W. Kwon, Distinguished Professor of Mechanical Engineering
   Naval Postgraduate School
   Monterey, California

4. Jarema M. Didoszak, Research Assistant Professor
   Naval Postgraduate School
   Monterey, California

5. Professor Yeo Tat Soon
   Temasek Defence Science Institute, National University of Singapore
   Singapore

6. Ms. Tan Lai Poh
   Temasek Defence Science Institute, National University of Singapore
   Singapore